



LUND UNIVERSITY

Synthetic strategies towards ether-free polymeric hydroxide conducting membranes

Mansouri Bakvand, Pegah

2025

Document Version:

Publisher's PDF, also known as Version of record

[Link to publication](#)

Citation for published version (APA):

Mansouri Bakvand, P. (2025). *Synthetic strategies towards ether-free polymeric hydroxide conducting membranes*. Department of Polymer Science & Engineering, Lund University.

Total number of authors:

1

General rights

Unless other specific re-use rights are stated the following general rights apply:

Copyright and moral rights for the publications made accessible in the public portal are retained by the authors and/or other copyright owners and it is a condition of accessing publications that users recognise and abide by the legal requirements associated with these rights.

- Users may download and print one copy of any publication from the public portal for the purpose of private study or research.
- You may not further distribute the material or use it for any profit-making activity or commercial gain
- You may freely distribute the URL identifying the publication in the public portal

Read more about Creative commons licenses: <https://creativecommons.org/licenses/>

Take down policy

If you believe that this document breaches copyright please contact us providing details, and we will remove access to the work immediately and investigate your claim.

LUND UNIVERSITY

PO Box 117
221 00 Lund
+46 46-222 00 00



Synthetic strategies towards ether-free polymeric hydroxide conducting membranes

PEGAH MANSOURI BAKVAND

CENTRE FOR ANALYSIS AND SYNTHESIS | LUND UNIVERSITY



Synthetic strategies towards ether-free polymeric hydroxide conducting membranes

Synthetic strategies towards ether-free polymeric hydroxide conducting membranes

Pegah Mansouri Bakvand



LUND
UNIVERSITY

DOCTORAL DISSERTATION

by due permission of the Faculty of Engineering, Lund University, Sweden.

To be defended at Kemicentrum, Lecture Hall K:A on March 7, at 9:30.

Faculty opponent

Dr. Naser Tavajohi
Umeå University

Organization: LUND UNIVERSITY Author(s) Pegah Mansouri Bakvand	Document name: Doctoral Dissertation	
	Date of issue 2025-03-07	
	Sponsoring organization	
Title and subtitle: Synthetic strategies towards ether-free polymeric hydroxide conducting membranes		
Abstract: <p>The only way to combat the depletion of resources and climate crisis is to reduce our dependence on fossil fuels. Renewable sources, such as wind and solar energy, are increasingly used to meet our ever-growing energy demands; however, they are intermittent. One promising solution to the power crisis in the world is fuel cells, which, unlike the combustion engine, can operate on renewable fuels such as hydrogen, methanol, and ethanol without emitting pollutants with high efficiency. A conventional type of polymer electrolyte fuel cell is proton exchange fuel cells (PEMFCs), which have already moved from laboratory to market; however, the usage of Pt catalyst makes them costly and unstable. On the other hand, the fuel cells operating in alkaline media, anion exchange membrane fuel cells (AEMFCs) can use nonprecious-metal catalysts with higher redox reaction kinetics. However, the technology of AEMFCs is currently less developed than that of PEMFCs due to several challenges, including the need for high-performing anion exchange membranes (AEMs) that can meet all requirements. The two main challenges hampering the development of AEMs for fuel cells are the lower conductivity of PEMs and the lower thermochemical stability in alkaline media. It is worth noting that research efforts now focus on obtaining stable polymer AEMs with high efficiency and low degradation in alkaline media.</p> <p>This thesis aims to investigate different structural factors, including polymer backbone, and the design and placement of cationic moieties on the final properties of AEMs. Several ether-free polymers were synthesized through superacid-mediated polyhydroxyalkylation reactions and, after required functionalization, were conducted to make fully quaternized polymers. AEMs were prepared from the polymers and investigated in terms of water uptake, ion conductivity, thermal properties, morphology, and alkaline stability.</p>		
Key words: anion exchange membrane, fuel cell, ether-free polymer, quaternary ammonium, alkaline stability, ion conductivity		
Classification system and/or index terms (if any)		
Supplementary bibliographical information		Language English
ISSN and key title		ISBN: 978-91-8096-098-4 (Print) 978-91-8096-099-1 (Digital)
Recipient's notes	Number of pages 73	Price
	Security classification	

I, the undersigned, being the copyright owner of the abstract of the above-mentioned dissertation, hereby grant to all reference sources permission to publish and disseminate the abstract of the above-mentioned dissertation.

Signature

Date 2025-01-22

Synthetic strategies towards ether-free polymeric hydroxide conducting membranes

Pegah Mansouri Bakvand



LUND
UNIVERSITY

Cover photo (front): A schematic image of the chemical structures of monomers used in this thesis, along with the process of peeling off the membrane from a Petri dish, by Zhili Cai.

Cover photo (back): Photograph of the Lund University main building, by Kennet Ruona (from LU image and media bank)

© Pegah Mansouri Bakvand

Paper I © the Authors (Open Access)

Paper II © the Authors (Open Access)

Paper III © the Authors (Open Access)

Paper IV © by the Authors (Manuscript unpublished)

Paper V © by Authors (Open Access)

Faculty of Engineering

Department of Chemistry, CAS


ISBN 978-91-8096-098-4 (Print)

ISBN 978-91-8096-099-1 (Digital)

Printed in Sweden by Media-Tryck, Lund University
Lund 2025



Media-Tryck is a Nordic Swan Ecolabel
certified provider of printed material.
Read more about our environmental
work at www.mediatryck.lu.se

MADE IN SWEDEN 

Dedicated to my parents and my husband, Amin

Abstract

The only way to combat the depletion of resources and climate crisis is to reduce our dependence on fossil fuels. Renewable sources, such as wind and solar energy, are increasingly used to meet our ever-growing energy demands; however, they are intermittent. One promising solution to the power crisis in the world is fuel cells, which, unlike the combustion engine, can operate on renewable fuels such as hydrogen, methanol, and ethanol without emitting pollutants with high efficiency. A conventional type of polymer electrolyte fuel cell is proton exchange fuel cells (PEMFCs), which have already moved from laboratory to market; however, the usage of Pt catalyst makes them costly and unstable. On the other hand, the fuel cells operating in alkaline media, anion exchange membrane fuel cells (AEMFCs) can use nonprecious-metal catalysts with higher redox reaction kinetics. However, the technology of AEMFCs is currently less developed than that of PEMFCs due to several challenges, including the need for high-performing anion exchange membranes (AEMs) that can meet all requirements. The two main challenges hampering the development of AEMs for fuel cells are the lower conductivity of PEMs and the lower thermochemical stability in alkaline media. It is worth noting that research efforts now focus on obtaining stable polymer AEMs with high efficiency and low degradation in alkaline media.

This thesis aims to investigate different structural factors, including polymer backbone, and the design and placement of cationic moieties on the final properties of AEMs. Several ether-free polymers were synthesized through superacid-mediated polyhydroxyalkylation reactions and, after required functionalization, were conducted to make fully quaternized polymers. AEMs were prepared from the polymers and investigated in terms of water uptake, ion conductivity, thermal properties, morphology, and alkaline stability.

Table of Contents

Abstract	i
Table of Contents.....	ii
Acknowledgments.....	iv
Popular science	vi
چکیده	viii
List of appended papers.....	ix
Abbreviations.....	xi
1 Context and scope.....	1
2 Introduction	2
2.1 Fuel cell.....	2
2.1.1 Proton exchange membrane fuel cells	3
2.1.2 Anion exchange membrane fuel cells.....	4
2.2 Anion exchange membranes	6
2.2.1 Water management, ion transport, conductivity, and morphology.....	7
2.2.2 Polymer backbone	8
2.2.3 Cationic group	9
2.2.4 Durability of AEMs.....	11
2.3 Approach and aim	12
3 Experimental methods	14
3.1 Synthesis	14
3.1.1 Polymer synthesis.....	14
3.1.2 Monomer synthesis.....	16
3.1.3 Polymer functionalization and quaternization.....	20
3.2 Characterization methods.....	21
3.2.1 Polymer characterization	21
3.2.2 Membrane preparation and characterization	23
4 Summary of appended papers.....	29
4.1 Paper I: Poly(arylene alkylene)s with pendant benzyl-tethered ammonium cations	29
4.2 Paper II: Tuning the properties of AEMs by changing the configuration of arene	32

4.3 Paper III: The effect of alkyl spacers in the alicyclic QA	35
4.4 Paper IV: <i>N</i> -Spirocyclic quaternary ammonium ionene	39
4.5 Paper V: zwitterionic poly(terphenylene quinuclidinium)	41
5 Conclusion and outlook.....	44
5.1 Conclusion.....	44
5.2 Outlook.....	45
6 References	46

Acknowledgments

I am deeply grateful to many people whose help and support during these years have been invaluable to me and made this journey possible.

First, I would like to thank my supervisor, **Patric**, for giving me this opportunity to do my research and studies in his group. *Patric*, your guidance, support, and encouragement have been priceless, and I have always appreciated the freedom you gave me to explore my own ideas. Your patience and open-mindedness in our discussions have been a constant source of inspiration. I am truly grateful for your role in supporting my growth as a researcher.

I would like to thank my co-supervisor, **Bao**, for having many constructive discussions regarding my studies. I would like to thank my previous and present CAS representatives **Lotta** and **Kenneth**, for their support. **Viveka**, thank you for the time and effort you devoted to discussing the various perspectives of being an international student at LTH and CAS.

I wish to express my gratitude to **Maria**, **Sara**, **Kornelije**, **Katarina**, and **Fatima** for their tireless efforts in solving problems and assisting with administrative affairs, instrument maintenance, and purchasing, all of which eased the challenges of research life. I would also like to thank everyone at the *Polymat group* and *CAS* for fostering a friendly and supportive environment.

A big thank you to my past and present colleagues in the *Polymer* and *Electrolyte Group*, whose support, insights, and collaboration have made a huge impact on my work. Thank you, **Isabell**, for your support, collaboration, and, more importantly, our friendly conversations, which gave me a space to share my thoughts. I truly enjoyed the time we spent working together in the lab. **Oskar**, thank you for proofreading my thesis and for your prompt help with various issues. **Zhili**, thank you for your constant positivity as both my lab- and office mate and for all your help with designing my cover image. **Olivier**, thank you for all our discussions and your support as my lab- and office mate. I also would like to thank **Haiyue**, **Anuja**, **Tam**, and **Xiaoting**, my other office mates, for making my workdays enjoyable and productive, as well as for maintaining a positive and supportive atmosphere. I would like to wish luck to new PhD students in our group, **Niloofer**, and **Jing**, as they embark on this exciting journey. Thank you, **Triet** and **Si**, for all your help, especially in the microscopy characterization. **Joel**, **Huong**, **Hannes** thanks for generously sharing your knowledge and experience. I have greatly benefited from the support of other group members, whose input has contributed to this thesis in numerous meaningful ways. I extend my thanks to **Andrit**, **Nitin**, **Sudhir**, **Dong**, **Niklas**, **Olga**, **Choi**, **Smita**, **Rafael**, **Sathiyaraj**, and **Yang**. To *Polymer* and

Electrolyte Group: I am truly grateful to have had the opportunity to know and work with you on this journey.

I was privileged to collaborate with outstanding researchers from KTH and Chalmers through the SSF-FFI project. I am grateful to **Carina, Göran, Rakel, Björn, Inna**, and the other researchers in the project for their valuable collaboration, and insights. I would like to thank you, **Amirreza**, for your constructive collaboration and idea-sharing throughout our project.

Beyond work, I was fortunate to make great friends in Lund who made my time there truly enjoyable and memorable. **Negar**, I am so happy I joined the Swedish course where we met and our friendship began. Thank you to both you and **Nicholas**, for being such supportive friends. **Laleh, Azin, Hediye, Najmeh, Rezvan, Mitra, Nikos, Peter, Peyman, Hesam, Vesal, Karina, Maria, Carlos**, and many others: it has truly been a pleasure knowing each of you, and I have always enjoyed the time we had together.

I would like to express my sincere gratitude to my dear friends back home in Iran. **Sahar** and **Sepideh**, you have always supported me, even though we are miles apart. Thank you for being there through many of my highs and lows. I would like to thank **Hanieh K., Neda, Sadaf, Pegah, Neda K., Hanieh T., Somayeh, Reza, and Behrad** for their valuable friendship. Their encouragement and thoughtful messages have been comforting throughout the last few years. I would like to thank **Iran**, for her advice during my academic struggles.

I would not be here without the unconditional support of my family by my side. My parents, **Parvin** and **Houshang**, whose love and belief have been the foundation of my journey, consistently encourage me to pursue my dreams. My wonderful sisters, **Shohreh, Goldis**, and **Sara**, are a constant source of support and strength. I am deeply thankful for everything you bring to my life. My sweet nephews, **Soroush** and **Borna**, bring immense joy to my life. My dear parents-in-law, **Mahnaz** and **Ali**, your support and kindness have always been a great encouragement, and I am deeply grateful. I would like to greatly thank the rest of my family for their support.

To my husband, **Amin**: words cannot fully express how grateful I am for your presence and support. From the start of our journey to this very day, your love, kindness, and patience have been my greatest strength. You believed in me often more than I believed in myself, giving me the courage to persevere. I will always cherish every moment we have shared together.

This thesis work was funded by Swedish Foundation for Strategic Research (SSF) and Swedish Energy Agency through the FFI program. The financial support from them and Kungliga Fysiografiska Sällskapet i Lund is highly appreciated.

Popular science

Polymers are everywhere in our world, from the natural fibers in plants to the synthetic materials in our clothes, electronics, and packaging. Polymers are large molecules built from repeating units that are not only versatile but can also be engineered, opening up applications in advanced technologies. Ionic polymers, a specialized class of polymers with charged groups enabling ion conduction, when processed into thin, transparent films called ion exchange membranes (IEMs), act as both barriers and conductors in sustainable energy conversion and storage technologies like fuel cells and water electrolyzers, which are at the heart of the transition to cleaner energy solutions.

The urgency to address climate change has never been clearer. Transitioning to renewable energy sources like wind and solar is essential, but these intermittent resources require efficient energy conversion and storage solutions. Hydrogen offers a compelling answer. This clean, energy-dense fuel can be produced through water electrolysis powered by renewable electricity and later used in fuel cells to generate electricity, water, and heat as a by-product with almost zero CO₂ emissions. This cycle is central to the emerging hydrogen economy, which contributes to decarbonizing industries and transforming global energy systems.

Fuel cells and water electrolyzers, both crucial to hydrogen-based technologies, rely on IEMs to separate electrodes and transport ions. Two types of IEMs, proton exchange membranes (PEMs) and anion exchange membranes (AEMs), serve distinct purposes. PEMs, which conduct positively charged protons, dominate current commercial applications. However, AEMs, which transport negatively charged hydroxide ions, are gaining attention due to their advantages under alkaline conditions. Alkaline systems can use less expensive, non-precious metal catalysts and operate with a broader range of fuels, making them more economical and versatile.

The performance and longevity of these devices highly depend on the quality of their IEMs. AEMs face significant challenges in alkaline environments, such as lower ionic conductivity and vulnerability to chemical degradation, especially at high hydroxide concentrations and elevated temperatures (80-100 °C). To overcome these limitations, researchers are designing new ionic polymers and membranes with improved stability and conductivity. Recent innovations involve tailoring the molecular architecture of AEMs to enhance their properties. These membranes typically consist of a hydrophobic polymer backbone for mechanical integrity and cationic groups that enable ion conduction. The type, arrangement, and density of these cations significantly impact conductivity and stability.

Identifying highly conductive and durable AEMs is essential for advancing the development and commercialization of alkaline fuel cells and water electrolyzer cells. This thesis utilized different methods to synthesize ionic polymers, which were then evaluated for their performance. The type and positioning of the cations were systematically varied to investigate their impact on the conductivity, water uptake, and stability of the resulting membranes. This research established crucial structure-property relationships, providing valuable insights for future research and development in AEMs.

چکیده

کاهش وابستگی به سوخت‌های فسیلی تنها راه مقابله با بحران اقلیمی و کاهش منابع طبیعی است. منابع تجدیدپذیر انرژی از قبیل باد و خورشید به طور فزاینده‌ای برای پاسخگویی به نیازهای رو به رشد انرژی مورد استفاده قرار می‌گیرند اما عدم دسترسی دائمی به این منابع به دلیل شرایط جوی، مشوقی برای یافتن راه‌حل‌های دیگر برای حل بحران انرژی شده است. یکی از راه‌حل‌های امیدوارکننده، سلول‌های سوختی هستند که برخلاف موتورهای احتراق داخلی، می‌توانند با استفاده از سوخت‌های تجدیدپذیر مانند هیدروژن، بدون انتشار آلاینده‌ها و با بازده بالا کار کنند.

یکی از انواع متداول سلول‌های سوختی با الکترولیت پلیمری، سلول‌های سوختی با غشای تبادل پروتون هستند که با عبور از فاز از مایشگاهی به بازار راه یافته‌اند. اما استفاده از پلاتین به عنوان کاتالیزور در این سلول‌ها و همچنین هزینه بالای تولید غشای پروتونی باعث افزایش هزینه‌ها و همچنین کاهش پایداری شده است. توسعه سلول‌های سوختی با غشای تبادل آنیون که امکان استفاده از فلزهایی با فراوانی بالا و غیرگران بها به عنوان کاتالیزور، مانند آهن و نیکل، دارد را میتوان راه‌حلی امیدوار کننده برای غلبه بر چالش‌های یاد شده در نظر گرفت. همچنین محیط قلیایی نسبت به محیط اسیدی خوردگی کمتری برای اجزای سلول سوختی ایجاد می‌کند. این نوع از سلول‌های سوختی که اساس کار آن تولید الکتریسیته از طریق واکنش اکسایش-کاهش در محیط قلیایی بوده، نیازمند طراحی و توسعه غشاهای تبادل آنیونی با کارایی و پایداری بالا است.

دو چالش اصلی که توسعه غشاهای تبادل آنیون برای سلول‌های سوختی را محدود می‌کنند عبارتند از: هدایت یونی کمتر نسبت به غشاهای تبادل پروتون و پایداری کم در محیط‌های قلیایی در دمای بالا. لازم به ذکر است که تلاش تیم‌های تحقیقاتی معطوف به طراحی و تولید غشاهای تبادل آنیونی با نرخ تخریب پایین و کارایی بالا شده است.

هدف این پایان‌نامه بررسی عوامل ساختاری مختلف، از جمله تأثیر زنجیر اصلی پلیمر، طراحی و جایگزینی گروه‌های کاتیونی، بر ویژگی‌های نهایی غشاهای تبادل آنیون است. چندین پلیمر با زنجیر اصلی فاقد اتر از طریق واکنش‌های پلی‌هیدروکسی‌آلکیل‌اسیون، با واسطه سوپراسید سنتز شده و پس از انجام مراحل عامل‌دار کردن، به زنجیره‌های پلیمری کواترنیزه تبدیل شدند. سپس این غشاهای اصلاح شده از نظر جذب آب، هدایت یونی در دماهای مختلف، خواص حرارتی، هدایت یونی، ریخت‌شناسی و پایداری در محیط قلیایی مورد بررسی قرار گرفتند.

List of appended papers

This thesis is based on the following papers

- I. Poly (arylene alkylene)s with pendent benzyl-tethered ammonium cations for anion exchange membranes.

Pegah Mansouri Bakvand, and Patric Jannasch,

Journal of Membrane Science, **2023**, 668, 121229

- II. Tuning the Performance of Poly (quaterphenyl piperidinium) Anion-Exchange Membranes by Monomer Configuration.

Pegah Mansouri Bakvand, Dong Pan, Andrit Allushi, and Patric Jannasch

Advanced Energy Material, **2024**, 2402869

- III. Polyfluorenes Bearing *N,N*-Dimethylpiperidinium Cations on Short Spacers for Durable Anion Exchange Membranes

Andrit Allushi,[†] Pegah Mansouri Bakvand,[†] and Patric Jannasch

Macromolecules, **2023**, 56, 1165–1176

[†] These authors contributed equally.

- IV. *N*-Spirocyclic quaternary ammonium ionene membranes prepared by polyhydroxyalkylation

Pegah Mansouri Bakvand, Thanh Huong Pham, and Patric Jannasch

In manuscript

- V. Highly alkali-stable zwitterionic poly(arylene quinuclidinium) anion exchange membranes

Pegah Mansouri Bakvand, and Patric Jannasch

Journal of Membrane Science, **2025**, 717, 123656

My contributions

- I. I planned and performed all the experimental work. I wrote the first draft of the paper.
- II. I planned and performed most of the experimental work. I wrote the first draft of the paper.
- III. I planned and performed half of the experimental work and contributed to writing half of the first draft.
- IV. I planned and performed a vast majority of the experimental work. I wrote the first draft of the paper.
- V. I planned and performed all the experimental work. I wrote the first draft of the paper.

Publications not concluded

- VI. Hydroxide ion conducting membranes dually functionalized with cationic and zwitterionic groups.

Anuja Shirole, Pegah Mansouri Bakvand, and Patric Jannasch

ACS Applied Energy Materials, **2023**, 6(13), 7240-7249.

- VII. Zwitterionic poly (terphenylene piperidinium) membranes for vanadium redox flow batteries.

Ivan Salmeron-Sanchez, Pegah Mansouri Bakvand, Anuja Shirole, Juan Ramón Avilés-Moreno, Pilar Ocón, Patric Jannasch, Rakel Wreland Lindström, and Amirreza Khataee

Chemical Engineering Journal, **2023**, 474, 145879.

- VIII. Hydroxide conducting BAB triblock copolymers tailored for durable high-performance anion exchange membranes.

Andrit Allushi, Pegah Mansouri Bakvand, Haiyue Gong, and Patric Jannasch

Materials Advances, **2023**, 4(17), 3733-3745.

- IX. Improving poly (arylene piperidinium) anion exchange membranes by monomer design.

Dong Pan, Pegah Mansouri Bakvand, Thanh Huong Pham, and Patric Jannasch

Journal of Materials Chemistry A, **2022**, 10(31), 16478-16489.

Abbreviations

FC	Fuel cell
IEM	Ion exchange membrane
AEM	Anion exchange membrane
HEM	Hydroxide exchange membrane
AFC	Alkaline fuel cell
AEMFC	Anion exchange membrane fuel cell
AEMWE	Anion exchange membrane water electrolyzer
WE	Water electrolyzer
PEM	Proton exchange membrane
PEMFC	Proton exchange membrane fuel cell
PGM	Platinum-group metals
QA	Quaternary ammonium
Qui	Quinuclidinium
TFA	Trifluoroacetic acid
TFSA	Trifluoromethanesulfonic acid
TFAp	Trifluoroacetophenone
SAXS	Small-angle X-ray scattering
DSC	Differential scanning calorimetry
DCM	Dichloromethane
NMP	N-Methyl-2-pyrrolidone
aq.	Aqueous

Symbols

$[\eta]$	intrinsic viscosity
σ	ion conductivity
d	characteristic distance
q	scattering vector
$T_{d,95}$	the temperature at 5% weight loss (by TGA)

1 Context and scope

The reliance on fossil fuels for global energy production has significantly contributed to greenhouse gas emissions, which are causing climate change impacts such as more intense heatwaves, frequent extreme weather events, rising sea levels, and loss of biodiversity.¹ Earth's average surface temperature is now about 1.2 °C higher than preindustrial levels in the late 19th century. Limiting the temperature rise to 1.5 °C is critical for maintaining ecological stability, which requires reducing greenhouse gas emissions by at least 45% of 2010 levels by 2030 and achieving net-zero emissions by 2050.¹ Achieving these targets requires a transition from fossil fuel-based energy to those powered by renewable energy sources.² However, while renewable energy sources such as wind and solar power are widely available and cost-effective, they are intermittent, seasonal, and geographically dependent.^{2, 3} As a result, the development of alternative energy technologies that would offer sustainable energy is essential to ensure a consistent energy supply.^{3, 4}

For instance, hydrogen (H₂) has emerged as a promising energy carrier due to its high energy density and ability to store and transport energy efficiently.⁵ Hydrogen can address large-scale energy storage and transportation challenges, either as compressed gas or in hydrogen-rich compounds.^{5, 6} However, for hydrogen to truly contribute to decarbonization, its production must also be carbon-neutral. Green hydrogen refers to H₂ produced via water electrolysis, where water is split into hydrogen and oxygen using renewable electricity, resulting in zero emissions.⁷ Additionally, fuel cells (FCs) convert the energy stored in fuel (e.g. hydrogen, methanol, etc.) into electricity through an electrochemical process with higher efficiency than combustion with almost no harmful pollutant emission.⁸ For example, when the fuel is H₂, they produce water and heat as byproducts.^{9, 10} These FCs are fundamentally the same, except for the electrolyte, which determines their operating temperature.¹¹⁻¹³ One type of FC is an AEMFCs in which a solid electrolyte membrane, an AEM, separates the two electrodes and transports hydroxide from the cathode to the anode.¹¹ The properties of these materials play a critical role in determining the efficiency, performance, and lifespan of the devices, and they are challenged by the high operating pH and temperature in the device.¹⁴ Due to these challenges, meeting the requirements of high ionic conductivity and structural integrity over thousands of hours is difficult to achieve.^{14, 15}

These technologies enable hydrogen to be stored as a chemical fuel and converted back into electricity with high efficiency, offering a pathway for reducing greenhouse gas emissions while meeting large-scale energy demands. Building on the recent findings and reports, this thesis explores the design, preparation, and analysis of AEMs, specifically used in alkaline media. The resulting membranes were then tested, with a particular emphasis on their chemical stability, to assess their suitability for applications.

2 Introduction

Ion exchange membranes (IEMs) are widely used in different electrochemical devices such as FC,¹⁶⁻¹⁸ water electrolyzers (WE),¹⁹⁻²¹ redox flow batteries²²⁻²⁴. IEMs are semi-permeable membranes that consist of ionic functional groups covalently attached to polymers, which can mainly be categorized into two primary classes based on the nature of conducted ions.²⁵ Membranes with negatively charged functional groups facilitate cation transport, predominantly protons, and are termed PEMs, while those with positively charged groups enable anion conduction and are classified as AEMs.^{17, 26}

In the upcoming sections, a brief discussion on FCs operating at temperatures below 90°C that utilize IEMs will be given. The focus will be on their fundamental operating principles, the advantages and limitations, and most importantly, the specific requirements for IEMs. Developments in other components, such as catalyst and diffusion layers, will not be covered, nor will systems that do not use IEMs as electrolytes be addressed. Particular emphasis will be placed on AEMs designed for alkaline environments, specifically hydroxide exchange membranes (HEMs), where hydroxide ions act as the conducting species. The discussion will include typical polymeric and cationic structures, membrane requirements, and especially chemical stability challenges in AEMs.

2.1 Fuel cell

The FC prototype was invented in the 19th century and has undergone significant development since then.²⁷⁻²⁹ FCs are systems that continuously transform the chemical energy of gaseous or liquid reactants into electrical energy through electrochemical processes.¹¹ FCs can operate as long as they are supplied with fuel and oxidant.³⁰ Furthermore, they produce energy with high conversion, and when the fuel is H₂, they produce water and heat with much less CO₂ emission (almost zero) in comparison to conventional fossil fuel-powered combustion engines.^{9, 10} FCs have applications in stationary, automotive, and stationary applications.^{31, 32} FCs based on H₂ have been reported to have a comparable driving range, refueling time, and lifetime to conventional cars with combustion engines.^{33, 34}

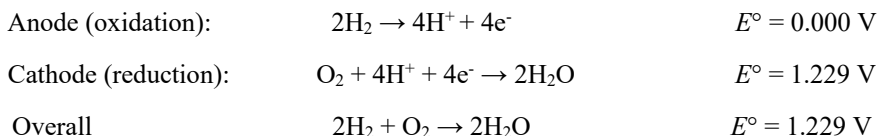
Basically, FCs consist of two electrodes, an anode, and a cathode, separated by an electrolyte and connected to an external circuit.^{11, 30, 35} In general, the oxidation reaction occurs at the anode, and electrons are generated while at the cathode, the reduction reaction occurs.^{11, 17, 30} With the flow of electrons, direct current electricity is produced through an external circuit between the anode and cathode. The type of ions produced in electrochemical reactions and their movement through the

electrolyte depends on the specific type of FC.^{10, 11, 17, 30, 35, 36} Over the years, a variety of FCs have been developed, typically classified based on the type of electrolyte used, which determines their operating temperature.^{11, 13} Some types of FCs include solid acid (SAFC),³⁷ phosphoric acid (PAFC),³⁸ solid oxide (SOFC),³⁹ molten carbonate (MCFC),⁴⁰ alkaline (AFC),⁴¹ and polymer electrolyte membrane fuel cell.^{11, 42} Polymer electrolyte membrane fuel cells can be divided into two main categories based on the operating conditions and the type of membrane used: PEMFC and AEMFC.⁴²

This thesis primarily focuses on developing AEMs for potential application in electrochemical devices operating in alkaline media like FC. Accordingly, this section provides a brief overview of these devices and outlines the specific requirements for AEMs in their applications.

2.1.1 Proton exchange membrane fuel cells

PEMFCs have become a competitive power source for stationary, automotive, and portable applications due to their high energy conversion efficiency, minimal emissions, rapid load response, and low operational temperature.⁴³ Most electric vehicles today rely on batteries, which work well for smaller cars and trucks under 5 tons; however, larger vehicles face challenges with battery weight and space constraints, making it difficult to meet range requirements. Therefore, FC-powered vehicles are essential, offering an emission-free and environmentally friendly solution for heavier or long-range applications.⁴⁴ The overall electrochemical reaction when the H₂ is used as fuel is described as follows:



The oxygen reduction reaction (ORR) at the cathode is kinetically slower at low temperatures (e.g., 80 °C), leading to a sluggish overall FC reaction. Using a highly active and stable catalyst, such as platinum (Pt), effectively lowers the activation energy and enhances the reaction rate.⁴⁵

Thanks to significant efforts, some progress has been made in replacing or decreasing the loading of Pt catalyst, but the high dependency of PEMFC on Pt-based catalysts, especially on the cathode side, is still limiting the widespread commercialization and further progress is necessary to make them as a viable alternative to combustion engines.^{45, 46} The most typical electrolyte to be used in PEMFC is a class of perfluorinated sulfonic acid (PFSA), which was invented by DuPont and known by the trademark Nafion. Nafion is a semicrystalline random copolymer consisting of a hydrophobic fluorinated backbone (typically polytetrafluoroethylene, PTFE) with randomly distributed sulfonic acid capped-

perfluoro ether side chains, as shown in **Figure 1**.⁴⁷ The intrinsic chemical dissimilarity between the covalently bonded ionic pendant groups and the hydrophobic PTFE backbone promotes microphase separation, which is further intensified by solvation upon the introduction of polar molecules such as water or other solvents.⁴⁷ For instance, Nafion 112 can reach around 0.09-0.1 S cm⁻¹ proton conductivity in a fully hydrated state at 25 °C.⁴⁸ Despite the high performance of Nafion, it has some limitations, including high cost, low performance at lower relative humidity, and low mechanical properties at elevated temperatures.^{49, 50} All the aforementioned drawbacks hamper the large-scale commercialization of FC vehicles.

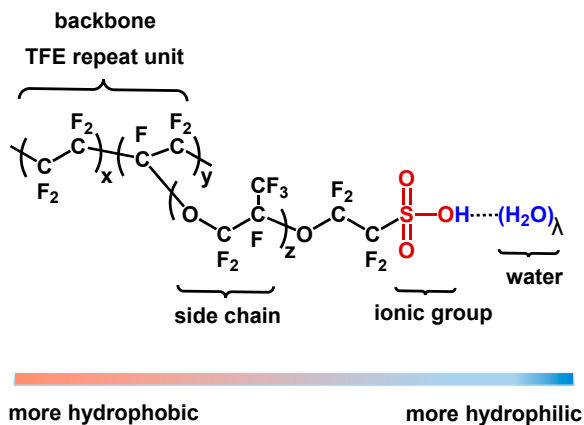


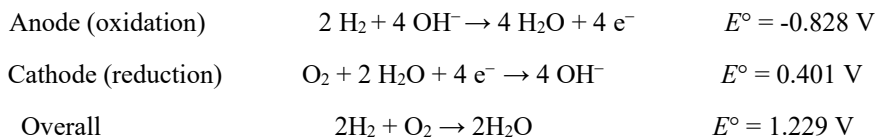
Figure 1. Chemical structure of Nafion (adapted from Kusoglu et al.).⁴⁷

2.1.2 Anion exchange membrane fuel cells

AEMFC is considered a new evolution of AFCs. AFCs were first invented at the beginning of the 20th century, and their development is closely tied to the space age.^{51, 52} The first generation of AFCs was made of KOH solution as an electrolyte, sintered nickel anode, sintered lithiated nickel/oxide cathode, and operated with pressurized gas (30-40 atm) at around 200 °C.⁵¹ Despite considerable success with space missions in 1960, AFCs have not been widely developed due to their electrolyte sensitivity to CO₂, which can consume hydroxide ions and lead to cell current reduction.⁵² Additionally, the formed carbonate can precipitate on the electrode and block gas diffusion. Furthermore, there is a higher possibility that the corrosive alkaline liquid electrolyte (KOH) leaks and destroys the system compared to the solid polymeric electrolyte implemented in modern FCs.⁴¹

FCs operating at alkaline conditions have advantages over the ones operating in acidic media, like faster reaction kinetics at the electrodes, which can result in higher cell voltage. This higher electrical efficiency enables the use of non-noble catalysts.^{53, 54}

Furthermore, alkaline media are less corrosive to cell components in comparison to acidic media. With advancements in membrane technology, replacing an alkaline solution of KOH (the common electrolyte) with AEMs was found to be effective in overcoming the challenges of AFCs.^{55, 56} The overall electrochemical reaction in an AEMFC when H₂ is used as fuel is described as follows:



Subsequently, increasing attention has been paid to AEMFCs due to their advantages over PEMFCs, including faster electrochemical kinetics, cost-saving catalysts, and stronger corrosion resistance. Moreover, the fuel feeding direction of AEMFC is opposite to the direction of ion transfer, which avoids the fuel leakage problem in FC.⁵⁷ The working principle of AEMFC closely resembles PEMFCs in structure and operation principles (**Figure 2**); however, several critical differences distinguish them, including the direction of ion transport, water management, and the presence of the OH⁻ ion, which acts as both a base and a nucleophile.⁴ For instance, one of the first solid AEMFCs without any doping of external base was reported in 2006 with 55 mW cm⁻² peak power density (PPD) at 50 °C,⁵⁶ and we have since seen substantial improvements. For example, norbornene-based tetrablock membrane with IEC around 3.8 mequiv g⁻¹ reached the highest reported PPD at the time of writing, up to 3.5 W cm⁻² at 80 °C.⁵⁸ It is important to note that these power densities are achieved under different conditions (temperature, catalyst type and amount, membrane thickness, etc.), which can significantly affect performance.

The technology of AEMFCs is currently lagging behind PEMFCs in technological maturity, mainly due to the lack of stability of cell components, including AEMs and catalysts, which can cause unrecoverable performance loss.^{42, 59} From an AEM perspective, various parameters play a role in the final performance, such as its chemical structure, ionic conductivity, water uptake, thermal and chemical stability, thickness, and mechanical properties, which can significantly impact cell performance. However, optimizing these parameters simultaneously is a significant challenge, as improvements in one area often come at the expense of another. For instance, enhancing ionic conductivity through increased ion exchange capacity can lead to excessive swelling and reduced mechanical stability. Consequently, developing AEMs that balance all these requirements while maintaining long-term stability in highly basic conditions remains a central focus of ongoing research efforts to advance AEMFC technology.

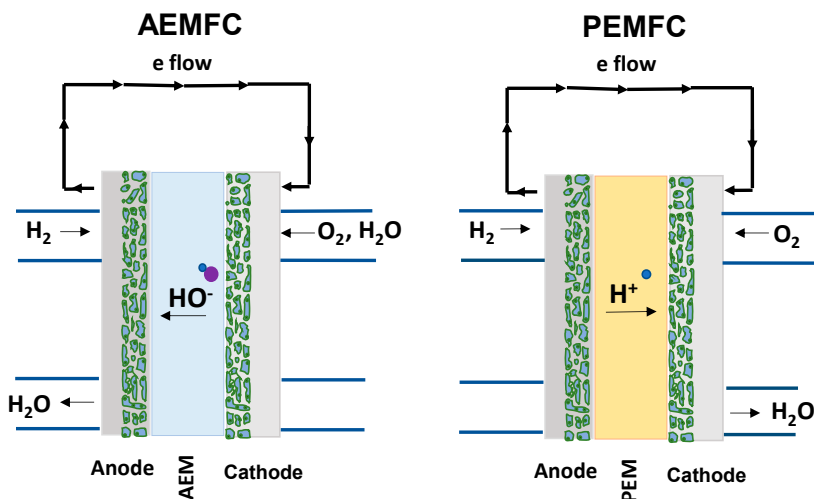


Figure 2. Schematic illustration of a PEMFC and AEMFC.

2.2 Anion exchange membranes

An AEM is made of polymeric structures covalently tethered with cationic groups, typically quaternary ammonium (QA), with OH⁻ as mobile counter ions. In other words, the AEM creates an alkaline environment inside the FCs.⁴² The aim of AEMs is to transport OH⁻ ions from the cathode to the anode while separating the anode and cathode to hinder fuel penetration, which can lead to internal short circuits, forcing electrons through the external circuit and insulating the electronics.⁶⁰ The requirements for efficient AEMs include high hydroxide conductivity, mechanical, thermal, and chemical stability, good separation properties, and moderate water uptake. It is also worth mentioning that the AEMs must be able to be readily produced on a large scale at a low cost.⁴ The two main challenges in implementing AEMs into FCs are the lower conductivity compared to PEMs and the lower chemical stability.⁵⁴ The lower conductivity compared to its competitor, PEM, can be correlated to the lower mobility of hydroxide ions in comparison to protons and the lower dissociation of cationic groups compared to anionic groups of PEMs at lower water content.^{9, 61} The insufficient conductivity can lead to low power and current densities. Increasing the number of cationic charges per gram of polymer, denoted as ion exchange capacity (IEC, mequiv g⁻¹) is the simplest way to address the low conductivity problem.^{60, 62} This strategy must be approached cautiously, which will be discussed in section 2.2.1.⁶²

The other major obstacle that needs to be addressed is the lower chemical stability of AEMs operating at high pH and elevated temperatures.⁶³ The hydroxide ions are

nucleophiles that can easily attack the cations or polymer backbone and jeopardize the chemical and mechanical stability of the membranes. Therefore, designing a stable structure for AEMs in order to survive in the alkaline environment is crucial.^{4, 9, 63}

2.2.1 Water management, ion transport, conductivity, and morphology

Ion transport in aqueous systems and ion exchange membranes primarily occurs through two mechanisms: vehicular diffusion and structural diffusion (Grotthuss mechanism).^{57, 64} The vehicular mechanism involves the movement of charged species along with their hydration shell, essentially "riding" on water molecules as they diffuse.⁶⁵ Structural diffusion, on the other hand, relies on the dynamic formation and interconversion of specific ionic structures. For protons, this involves Eigen (H_9O_4^+) and Zundel (H_5O_2^+) cations.⁶⁶ The relative contributions of these mechanisms can vary significantly depending on the system and conditions. Hydroxide transport is more complex than simply being the reverse of proton transport or a "proton hole" concept.⁶⁶ OH^- ions are typically hypercoordinated, accepting about 4-4.5 hydrogen bonds in a square-planar arrangement, compared to the protons interacting with only 2-3 water molecules.⁶⁷ The different mechanism, involving additional hydrogen bond rearrangements plus reorientations, is the reason for the reduced mobility of the hydroxide ion compared with the oxonium ion. For instance, conductivity measurements clearly show that the mobility of $\text{H}^+(\text{aq})$ ($36.23 \times 10^{-8} \text{ m}^2/(\text{s V})$) is significantly higher than that of $\text{OH}^-(\text{aq})$ ($20.64 \times 10^{-8} \text{ m}^2/(\text{s V})$) at room temperature.⁶⁶ Consequently, the diffusion coefficients derived from these mobilities are $9.31 \times 10^{-9} \text{ m}^2/\text{s}$ for $\text{H}^+(\text{aq})$ and $5.30 \times 10^{-9} \text{ m}^2/\text{s}$ for $\text{OH}^-(\text{aq})$.⁶⁶ It has been reported that the mechanism for hydroxide transport is highly dependent on the hydration state; e.g., the vehicular mechanism often contributes more to hydroxide transport than structural diffusion, especially at lower hydration levels.⁶⁴ Another factor that causes the higher conductivity of proton is the higher degree of dissociation of sulfonic group even at a lower hydration level ($1 < \lambda < 2 = 19\% \text{ RH}$)⁶⁸ in comparison to QA.⁶⁷ This phenomenon can be correlated to the fact the sulfonic acid groups are strong acids with $\text{pK}_a \sim -3$ while the QA group considers weak bases with $\text{pK}_b \sim 4$ (conjugate acid $\text{pK}_a > 10$).^{64, 69} Additionally, the susceptibility of alkaline systems to CO_2 contamination leads to the formation of carbonate ion species (CO_3^{2-} and HCO_3^-).⁷⁰ These ions have lower mobility than hydroxide ions and can accumulate in the membrane, further reducing overall ionic conductivity and potentially degrading membrane performance over time.⁷⁰ AEMs typically require higher IEC and better hydration than PEMs to achieve comparable performance. Increasing the IEC to address the low conductivity problem is the most straightforward approach.⁶⁰ By increasing IEC, the concentration of cationic groups will increase, leading to higher water uptake, which is essential for forming percolating water-rich channels.⁶² This strategy must be used with caution, as extensive water uptake causes cation dilution and decreases in conductivity. Additionally, excessive water uptake can result in a high degree of

swelling and deterioration of the mechanical properties.⁶² For instance, one possible way to enhance the conductivity without sacrificing the mechanical properties is by promoting phase separation through different methods, e.g., using alkyl extenders or spacers,⁷¹⁻⁷³ grafting multicationic side chain,⁷⁴ and block copolymerization.^{75, 76} Effective phase separation between hydrophobic polymer backbones and hydrophilic cations may be crucial for creating interconnected conducting channels.^{75, 76} The formation of ionic clusters in membranes may improve percolation and conductivity, even under conditions of low water uptake, compared to membranes lacking phase separation.⁷² In some cases, crosslinking was reported as an effective way to optimize water uptake, potentially leading to improved conductivity and enhancing mechanical properties.⁷⁷ However, the degree of crosslinking needs to be balanced since a high degree of crosslinking can lead to a low level of water uptake and ion transportation.⁷⁸ Recent advances have significantly improved the hydroxide ion conductivity of AEMs, bringing their performance closer to that of PEMs. However, achieving high conductivity while maintaining low water uptake remains a challenge. Addressing this issue requires a combination of high IEC, innovative polymer design, and the use of high molecular weight polymers.

2.2.2 Polymer backbone

Besides providing structural integrity and mechanical strength, polymer backbones also play a significant role in chemical stability.^{79, 80} Polymer chains can be cleaved due to the chemical degradation of the backbone, causing their molecular weight to decrease and destroying the mechanical strength.⁸⁰⁻⁸² This also can result in the breakage of membranes and, eventually, device failure.^{83, 84} AEMs were preliminary prepared through chemical modification of sulfonic acid groups in Nafion to QA group,⁸⁵ or through post-polymerization modification, like chloromethylation of PS,⁸⁶ or benzyl-bromination or -chlorination of polymers like poly(aryl ether sulfone)s (PSU),^{87, 88} and poly(*p*-phenylene oxide) (PPO),⁸⁹ and grafting on poly(vinylidene fluoride) (PVDF).⁹⁰ Later, studies showed limitations in the polymer backbone stability of these polymers. For instance, difluoroethylene is sensitive to high pH values where it undergoes dehydrofluorination.⁵⁵ Moreover, aryl-ether cleavage was reported for the AEMs based on PSU and PPO, which resulted in brittleness and failure of these membranes.⁹¹⁻⁹³ Further studies have shown that the barrier height of aryl-ether cleavage via the S_NAr reaction pathway generally decreases with the presence of more electron-withdrawing substituents on the phenyl group.⁹⁴ Different model compounds mimicking the PSU repeat unit showed different degrees of C–O bond cleavage near sulfone linkage. For example, almost complete degradation was reported for ortho-substituted benzyltrimethylammonium molecules in 4 equiv. of NaOCH₃ in DMSO-*d*₆/CD₃OD at room temperature for 20 h, while the ortho-substituted methyl one showed around 30% aryl ether cleavage.⁹⁵ However, no backbone degradation was reported for

aromatic polymers without aryl ether bonds, even for brominated trifluoromethyl-containing poly(biphenylalkylene) (PBA), which contained $-\text{CF}_3$ and $-\text{Br}$ in the structure due to the absence of sensitive aryl ether bond in the structure.⁹⁵ Various polymerization techniques have been developed to synthesize ether-free aromatic polymers with enhanced properties including metal-catalyzed coupling reactions for poly(phenylene-fluorene)s,⁹⁶ superacid-mediated polyhydroxyalkylations for poly(arylene alkylene)s (PAA),⁹⁷⁻⁹⁹ Diels-Alder polymerizations for poly(phenylene)s,^{100, 101} and cyclopolycondensation for spiro-ionenes.¹⁰² Each method offers distinct advantages, allowing researchers to tailor polymer structures for specific applications in various fields. Different representative polymer structures are shown in **Figure 3**. The mentioned polyaromatic ether-free structures typically exhibit enhanced thermal stability. Furthermore, the hydrophobicity of aromatic rings can possibly decrease the water uptake.

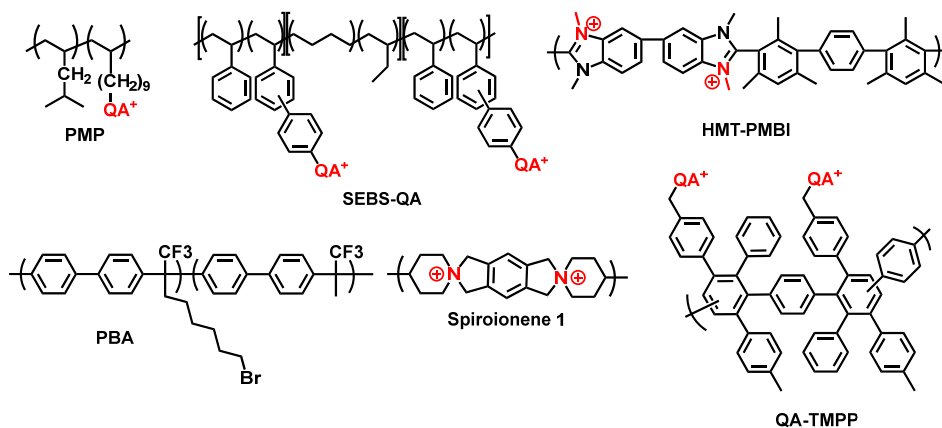


Figure 3. Examples of molecular structures of AEMs based on quaternized ether-free polymers.

2.2.3 Cationic group

Another difficult challenge in designing AEMs is identifying the most stable cation to embed in the structure. All the cationic groups that have been used in the polymer structures can generally be divided into N-containing,¹⁰³⁻¹⁰⁵ N-free,^{106, 107} and organic metal groups.^{108, 109} Examples of cationic groups are displayed in **Figure 4**.

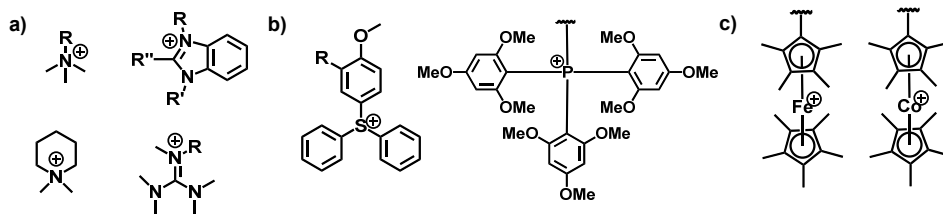


Figure 4. Representative molecular structure of N-containing (a), nitrogen-free (b), and organometallic (c) cationic groups.

Among all types of cations, QAs are typically preferred due to their accessibility, easy synthesis pathway, and easy way to attach them to the polymer structure.¹¹⁰ However, many QAs are prone to degradation through different pathways based on their structure.^{25, 111} The main degradation pathways include nucleophilic substitution on an α -carbon and Hofmann β -elimination, although other mechanisms may occur depending on the chemical structure of cations. Examples of degradation mechanisms are given in **Figure 5**.

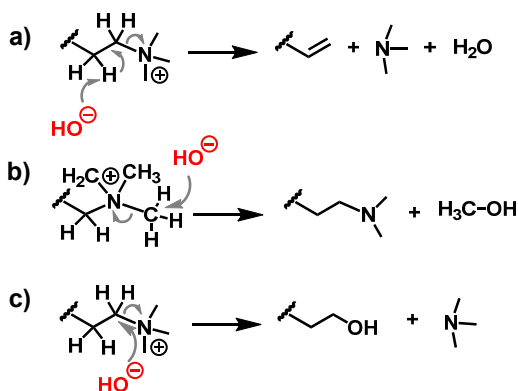


Figure 5. Degradation mechanism of acyclic QA through Hofmann β -elimination (a), and nucleophilic substitution (S_N2) at α -carbons (b, c).

Moreover, it was found that the placement of cations also plays an important role in their stability. For instance, it was reported that tethering the cations on the benzylic positions or nearby electron-withdrawing groups increases degradation significantly. Recently, it was found that the stability of QAs also depends on the microsolvation of hydroxide ions in the media, which defines the chemoselectivity of the hydroxide ions.^{112, 113} Hence, the chemoselectivity of the hydroxide ion to attack β -hydrogen, leading to an E_2 reaction, is favored at a lower microsolvation state due to the lower energy required for the transition state, as compared to the

attack on the carbon leading to S_N2 reaction.¹¹² In other words, the nucleophilicity and basicity of the hydroxide ions are affected by their degree of solvation. Thus, efforts have been made to design AEMs in ways to increase stability.¹¹¹ These strategies include the implementation of conformational restriction, steric hindrance, β -hydrogen free, and resonance and inductive effects in cations.¹¹⁴ Kreuer and Marino reported the stability of 26 QA cations in 6 M aq. NaOH at 160 °C. This study showed that alicyclic QAs like N,N-dimethylpiperidinium (DMP), and 6-azonia-spiro[5.5]undecane (ASU) possess the longest half-life in comparison to the rest of the studied QAs. This higher stability can be attributed to the higher activation energy needed for the deformation of the stable 6-membered rings.¹¹⁵ Furthermore, DMP cation degrades primarily through nucleophilic substitution at the methyl group, while the ASU cation shows higher stability due to its lack of methyl groups.¹¹⁵ The mentioned results were based on model compounds; however, the outcomes could vary upon incorporating cyclic QAs into the polymeric structure. The mentioned results have motivated many researchers to implement these cations in the structure of AEMs as the cationic moieties. Some possible degradation pathways for DMP and ASU are presented in **Figure 6**.

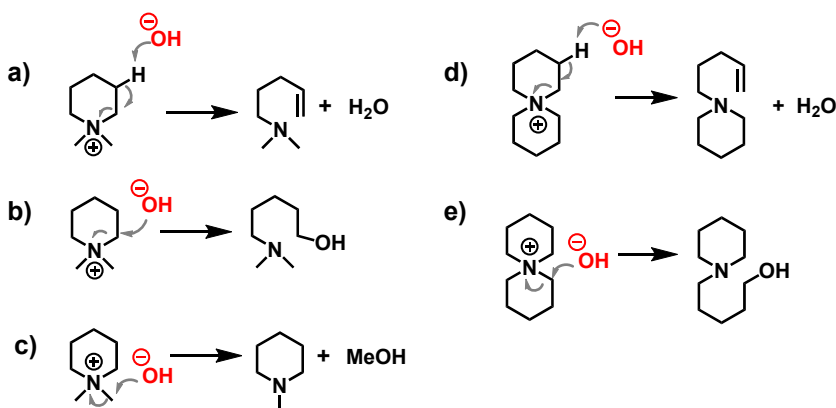


Figure 6. Possible degradation mechanisms of alicyclic QAs, DMP, and ASU by hydroxide ions through Hofmann β -elimination (a,d), nucleophilic substitution at α -carbon (b, c, e).

2.2.4 Durability of AEMs

As illustrated earlier, the stability of AEMs depends highly on the polymer backbone, the structure of the QAs, and the placement of QAs on the polymer backbone.^{18, 25, 81, 116, 117} It was found that the ether-free polymer backbone can improve alkaline stability.^{25, 81} However, due to the complexity of degradation mechanisms in polymers, an alkali-stable model compound does not necessarily ensure an alkali-stable AEM. Although the earlier studies on model compounds

reported high alkaline stability for alicyclic QAs,^{115, 118} the alkaline stability data of quaternized polymer may yield different results. For instance, the alkaline stability data on poly(terphenyl piperidinium) showed the Hofmann β -elimination as the preliminary degradation, which contrasts with the behavior of the small molecule model cation, where methyl substitution was the predominant degradation mechanism.^{115, 119} This phenomenon was attributed to the rigidity of the *p*-terphenyl based polymer backbone, which can distort the cation ring conformation and, as a result, lower the activation energy for degradation reactions and ultimately reduce stability in alkaline environments.¹¹⁹ Different strategies have been used to improve the stability of the AEMs, including crosslinking,¹²⁰⁻¹²² tethering flexible spacer,¹²³ and the incorporation of moieties with multiple cationic sites.¹²¹ Moreover, the mechanical properties can be improved by crosslinking,^{120, 122} reinforcement,¹²⁴ and blending.¹²⁵

In-situ durability evaluations of AEMs present significant challenges due to the complex operating environments encountered in applications.¹²⁶ These evaluations are further complicated by some factors including, but not limited to, variations in hydration levels, which affect dimensional stability and ion conductivity; pressure fluctuations, which can cause physical degradation over time; and the presence of reactive oxygen species, which may lead to chemical degradation of the membrane material.^{126, 127} For example, the oxidative degradation resistance of AEMs has been less extensively studied compared to other degradation mechanisms despite its critical role in ensuring long-term performance and durability in applications such as FCs and electrolyzers.^{81, 128} Addressing these challenges is essential to enhance the reliability and longevity of AEMs in practical settings.

2.3 Approach and aim

Building upon previously established concepts and extending earlier investigations into the influence of polymeric structure on material properties, this work aimed to develop novel polymer-cation arrangements for the fabrication of AEMs and evaluate their performance. Starting with alkali-stable polymer backbones and cations identified from the literature and previous work in our group, all polymers were designed and synthesized through superacid-mediated polyhydroxyalkylation and subsequent post-functionalization (**Figure 7**). While the synthetic process was designed to be straightforward, the creation of new monomers was occasionally required to achieve the targeted polymer architecture. The synthesized polymers were then cast into membranes and analyzed for key properties, including water uptake, ionic conductivity, thermal stability, and chemical resistance.

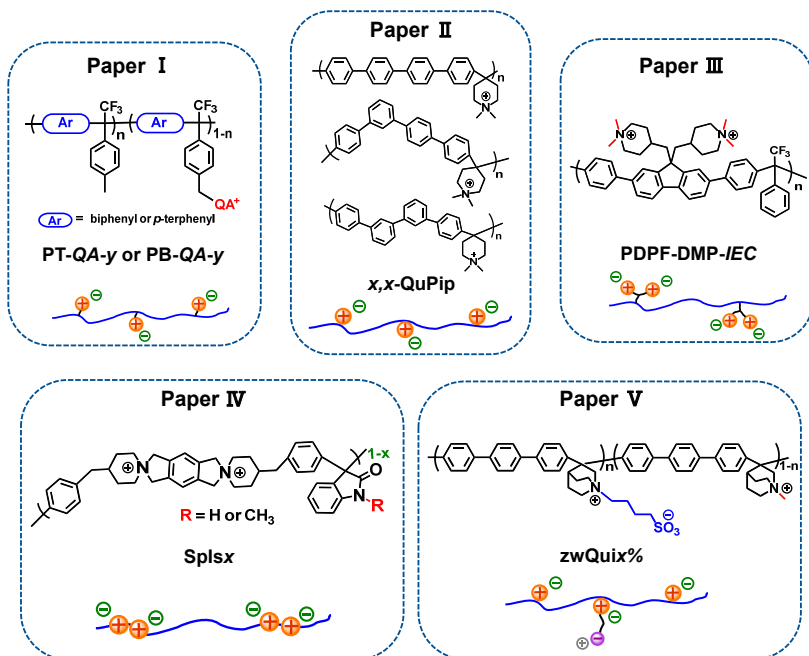


Figure 7. Summary of the thesis work in the form of polymer structures in the discussed appended papers.

3 Experimental methods

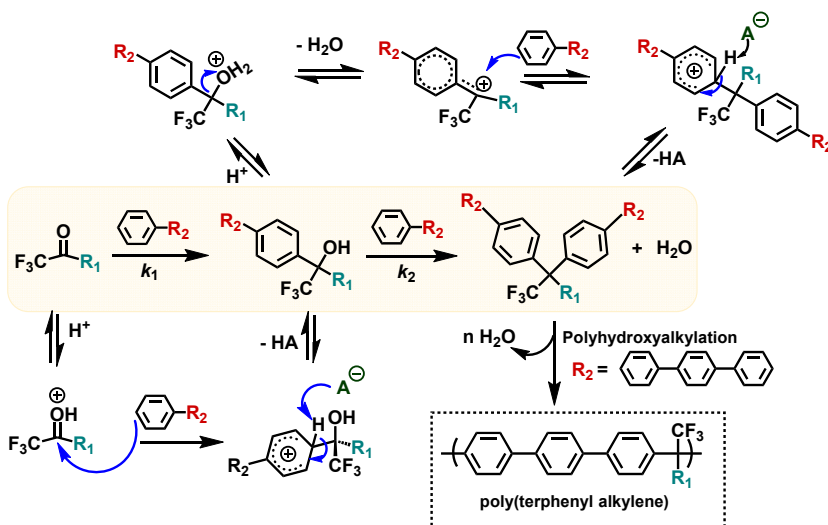
This chapter introduces the main experimental methods employed throughout the thesis. It is divided into two parts focusing on the different strategies employed to synthesize the cationic polymers and the characterization methods.

3.1 Synthesis

3.1.1 Polymer synthesis

In this thesis, the polymerization techniques are based on superacid-mediated polyhydroxyalkylation reactions. The term "hydroxyalkylation" traditionally describes Friedel-Crafts-type condensation reactions between aldehydes or ketones and electron-rich arenes under acidic conditions, leading to the formation of carboxonium ion intermediates. In certain cases, these intermediates can undergo further activation by strong Brønsted or Lewis acids, resulting in the formation of highly reactive dicationic species known as superelectrophiles.^{129, 130} This concept of superelectrophilic activation, introduced by Nobel Laureate George Olah and collaborators, has since proven highly effective in facilitating the synthesis of condensation monomers and polymers.¹²⁹⁻¹³³ A representative hydroxyalkylation reaction mechanism is presented in **Scheme 1**.

Scheme 1. Mechanism of the hydroxyalkylation reaction of an arene and a ketone in acid media. k_1 and k_2 are reaction constants.



In superacidic media, such as trifluoromethanesulfonic acid (TFSA), the reaction occurs in two sequential steps, and each step has been assigned its own rate constant (k_1 and k_2).^{134, 135} First, the superacid protonates the carbonyl group, an electrophile, which then undergoes condensation with an arene, producing a carbinol intermediate. In the subsequent step, the C-O bond of the carbinol breaks hydrolytically, generating a carbocation that reacts with a second arene. The ratio between rate constants (k_1/k_2) for these two steps is influenced by the structure of the reactants and the reaction conditions. The k_1/k_2 ratio is influenced by three factors: the electrophilicity of the carbonyl component, acid strength, and the nucleophilicity of the aromatic component. For instance, k_1 depends on the electrophilicity of the carbonyl group, as well as the strength of the acid and the reactivity of the aromatic component. Additionally, an increase in the nucleophilicity of the arene enhances both k_1 and k_2 by stabilizing the carbocation in the second step. The rate constants are also influenced by the acidity of the reaction medium; for example, an increase in the acidity of the reaction medium, while keeping all other factors constant, reduces k_1 at the expense of the protonation energy, while k_2 remains unaffected.¹³⁴ A study based on the model reaction of 2,2,2-trifluoro-4'-methoxyacetophenone with anisole was reported that when TFSA/Ketone would be equal, only diaryl product was formed; however, by increasing TFSA/ketone ratio to above 7 the monoaryl carbinol started to appear in quantitative yield.¹³⁵

Zolotukhin et al. reported the first applications of hydroxyalkylation chemistry to polymer synthesis and, in particular, to the synthesis of a new class of aromatic polymers, the polyaryleneoxindoles, by using isatin as a ketone.¹³³ Since then, this polymerization method has significantly broadened, enabling the synthesis of a diverse range of polymers from various carbonyl and aromatic compounds.^{19, 136-141} This type of polymerization process is highly efficient and can yield high molecular weight products when using a stoichiometric ratio of monomers. However, it has been observed that the polymerization rate significantly increases with an imbalanced monomer feed ratio, specifically when the ketone monomer is in excess and $k_1 < k_2$.^{134, 141} An imbalanced feed also produces polymers with higher molecular weights, which is particularly advantageous for AEMs precursor applications. However, an excessive amount of carbonyl monomer can result in crosslinked, insoluble polymers due to side reactions.¹³⁴

Ketone monomers containing electron-withdrawing substituents, such as trifluoromethyl ($-\text{CF}_3$) groups, are particularly promising for use in polyhydroxyalkylation reactions. The strong inductive effect of the $-\text{CF}_3$ group increases the electrophilicity of the carbonyl carbon, making it more susceptible to nucleophilic attack. This enhanced electrophilicity lowers the activation energy required for forming the carboxonium ion intermediate, thereby facilitating the reaction and increasing polymerization rates, which can lead to the formation of higher molecular weight polymers. Moreover, the incorporating $-\text{CF}_3$ groups

improves the thermal stability and elevates the glass transition temperature (T_g) of the resulting polymers. However, the effect of $-CF_3$ on reaction kinetics requires careful optimization. When both vicinal positions adjacent to the carbonyl group are substituted with $-CF_3$, the activation energy required for C-O cleavage increases drastically due to the destabilization of the intermediate carbocation, dramatically slowing the reaction rate and rendering the system nearly unreactive. On the other hand, substituting these positions with electron-donating groups such as methyl ($-CH_3$) causes the first step to have a much higher activation energy than the second, leading to the formation of unreactive intermediates and no progress on the reaction. Thus, while $-CF_3$ groups offer significant advantages in terms of reactivity and polymer properties, their impact on the reaction mechanism must be carefully considered.

Heterocyclic ketones, such as piperidone and quinuclidone, are commonly employed in superacid-mediated polyhydroxyalkylation reactions alongside trifluoroketones. Studies on model compounds indicate that the carbonyl groups in piperidone are more electrophilic than those in acyclic ketones.¹⁴²⁻¹⁴⁴ In the presence of acid, unfavorable through-space charge-dipole interactions occur between the positively charged ammonium group and the partial dipole of the carbonyl, destabilizing the ketone.^{145, 146} However, this destabilization is mitigated by nucleophilic addition. Additionally, ring strain in 4-heterocyclohexanones further enhances their reactivity compared to acyclic ketones, as the strain is relieved through a nucleophilic attack on the carbonyl, resulting in sp^3 hybridization.^{145, 146} Moreover, the protonated amine functions as an electron-withdrawing group through inductive effects, further increasing the electrophilicity of the carbonyl group.¹⁴⁵ Piperidones and quinuclidone have been used in the preparation of linear or hyperbranched polymers by condensation with e.g., biphenyl, terphenyl, and derivatives of fluorenes.^{98, 99, 119, 147-149}

3.1.2 Monomer synthesis

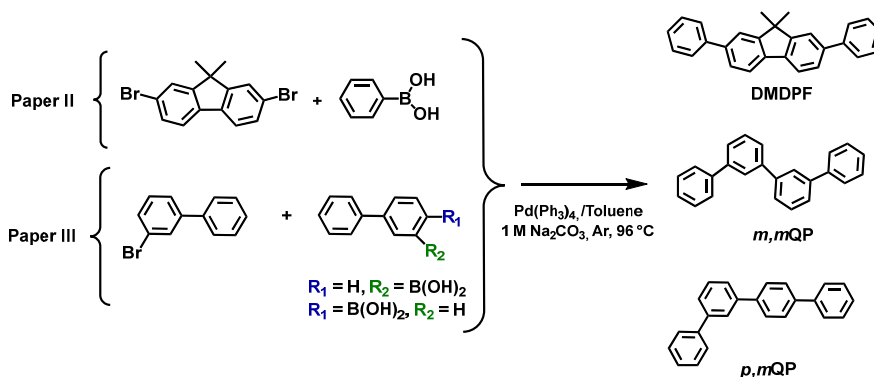
Non-ionic monomer

In Papers II and III, the non-ionic monomers were synthesized through Suzuki coupling reaction according to the previously published papers (**Scheme 2**).^{99, 150} The palladium-catalyzed cross-coupling reaction progresses through three interconnected steps.¹⁵¹ First, in the oxidative addition step, the palladium catalyst in its Pd(0) state inserts into the bond between the electrophilic halide (e.g., an aryl halide) and its leaving group, forming a Pd(II) complex. This is followed by transmetalation, where the organoboron reagent transfers its organic group to the palladium center, facilitated by a base that activates the organoboron compound and promotes ligand exchange. Finally, in reductive elimination, the palladium complex couples the two organic groups, forming the desired carbon-carbon (C-C) bond and regenerating the Pd(0) catalyst, completing the catalytic cycle.¹⁵¹

The synthesis procedure used for dimethyldiphenyl fluorene (DMDPF) is given as an illustrative example. 7,7-Dibromo-9,9-dimethyl-9H-fluorene was dissolved in toluene with phenylboronic acid and 1 M aq. Na_2CO_3 solution. After 4 vacuum/argon cycles to degas the mixture, $\text{Pd}(\text{PPh}_3)_4$ was added, and the reaction was refluxed under argon for 48 hours. The reaction was monitored by TLC using EtOAc: n-heptane (1:5). The mixture was then cooled, extracted with DCM, washed with brine, and dried over MgSO_4 . After filtering through a silica plug, the solvent was evaporated, and the crude product was purified by dry vacuum column chromatography using a heptane-toluene gradient. DMDPF was obtained as white crystals with 60% yield.

In Paper III, the same procedure was used to synthesize *para,meta*-, and *meta,meta*-quaterphenyl, *p,mQP*, and *m,mQP*, respectively, using 4-biphenylboronic acid or 3-biphenyl boronic acid with 3-bromo-1,1'-biphenyl (Scheme 2).

Scheme 2. Schematic route to arenes in Paper II, and III through aryl Suzuki coupling.

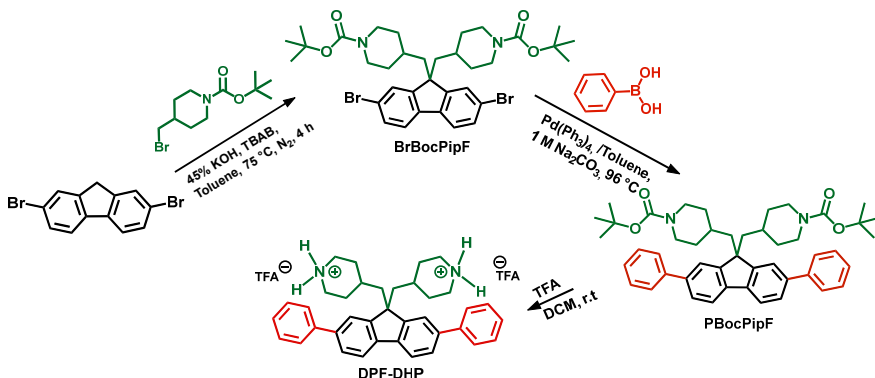


Cationic arenes

In Papers III and IV, the cationic arenes were synthesized. In Paper II, the dual piperidine rings were tethered to a fluorene-based monomer (**Scheme 3**). Fluorene possesses a rigid planar structure with two weakly acidic protons (C9-H) in the methylene bridge, which allows the introduction of different functional groups via alkylation reactions. This was achieved using a simple $\text{S}_{\text{N}}2$ alkylation reaction. Through alkylation reaction, two N-protected 4-bromomethylpiperidines were attached to the 9-position on dibrominated fluorene monomers in the presence of KOH as base and TBAB as a phase transfer catalyst in toluene under nitrogen atmosphere at 75 °C.^{99, 152} After cooling to room temperature, the mixture was extracted with DCM, and the organic layer was washed with brine and dried over MgSO_4 . Solvents were removed using a rotary evaporator. The crude product was purified by dry vacuum column chromatography. The product, BrBocPipF, was

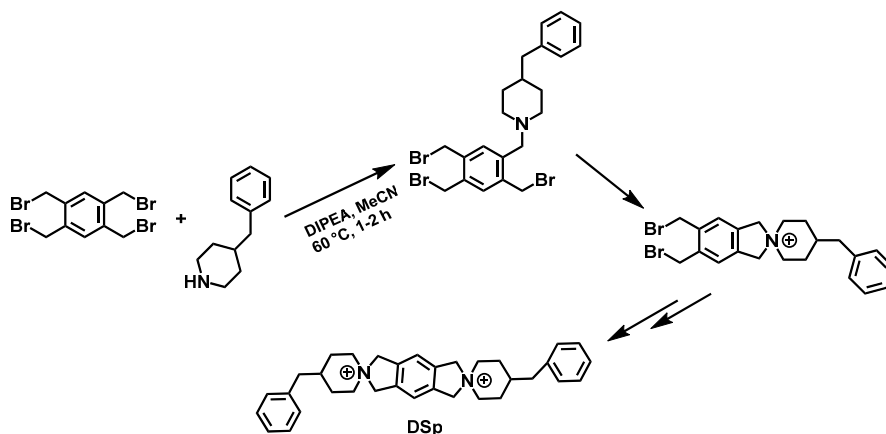
obtained. The same method was used to synthesize di-tert-butyl-4,4'-[(9H-fluorene-9,9-diyl)bis(methylene)]bis(piperidine-1-carboxylate) (BrBocPipF) with using fluorene. Next, BrBocPipF was diphenylated through Suzuki coupling, which was described before, to produce PBocPipF. In order to remove the Boc protection group, PBocPipF was dissolved in DCM. Then, TFA was added, and the mixture was stirred at room temperature for 4 hours. After evaporating the solvent, the product (DPF-DHP) was obtained as a white powder. The same method was used to deprotect BocPipF, yielding F-DHP as a white powder. After each step of modification, the molecular structures were verified using ^1H NMR spectroscopy.

Scheme 3. Synthetic route toward DPF-DHP in Paper III.



For Paper IV, the arene monomer containing two cyclic QA, 4,4''-dibenzyl-5',7'-dihydro-1'H,3'H-dispiro[piperidine-1,2'-pyrrolo[3,4-f]isoindole-6',1''-piperidine]-1,6'-dium (DSp), was synthesized through cycloquaternization of tBMB containing pairs of adjacent benzyl bromides with 4-benzyl piperidine (**Scheme 4**). This reaction involves two consecutive nucleophilic substitutions. The secondary amine first replaced one benzylic bromide group, forming a substituted intermediate through S_N2 reaction. The nitrogen then attacks the second bromomethyl group in an intramolecular reaction, leading to the formation of a cyclic QA structure.

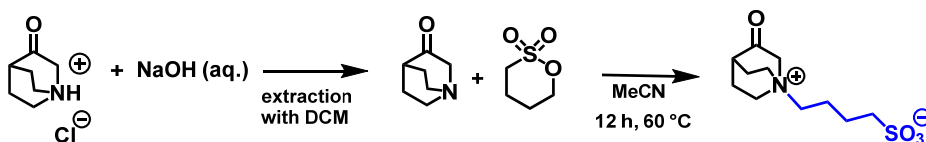
Scheme 4. Synthetic route toward DSp monomer in Paper IV.



Ketones

In Paper V, a ketone was synthesized. Recently, papers have been published that utilized 3-quinuclidone instead of piperidone as a ketone and reported significantly higher stability than PAPs.^{149, 153} These findings inspired the design of a zwitterionic monomer based on quinuclidinium to further improve alkaline stability (**Scheme 5**). For this purpose, a zwitterionic *N*-sulfobutylquinuclidinium-3-one, was synthesized through S_N2 reaction to develop the alkaline stability of our previous work we published on zwitterionic poly(terphenyl piperidinium)s.¹⁵⁴ First, 3-quinuclidinone hydrochloride was neutralized in 40 mL of aqueous NaOH and extracted with DCM. The organic phase was dried with $MgSO_4$, and the solvent was removed by rotary evaporation. Subsequently, the neutralized monomer was dissolved in MeCN, followed by the addition of 1,4-butanediol sulfonate and heating to 60 °C. A whitish solid formed within minutes and the mixture was refluxed overnight. After cooling, the solid product was filtered, washed with fresh MeCN, and recrystallized in methanol before drying in a vacuum oven, yielding 72%. The molecular structure was verified by 1H NMR spectroscopy.

Scheme 5. Synthetic route toward zwitterionic ketone, zwQui, in Paper V.



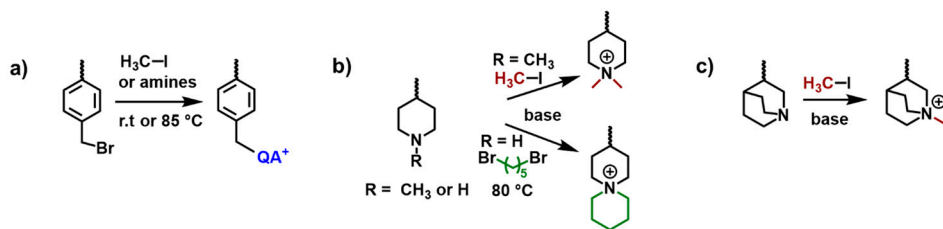
3.1.3 Polymer functionalization and quaternization

A key characteristic of the cationic polymers described in this thesis is their functionalization with QA cations. The incorporation of QA cations, commonly referred to as quaternization, is a central process throughout this work. In most cases, the QAs were introduced into the polymer chains via post-modification, except in Paper IV, where the quaternized monomer was first synthesized and subsequently polymerized through polyhydroxyalkylation. Notably, in Paper V, sulfoalkylated quinuclidone (zwQui) was also used in the copolymerization with 3-quinuclidinone hydrochloride, with full quaternization achieved in a subsequent step. In Paper I, the benzylic positions of polymers were brominated first through Wohl-Ziegler using N-bromosuccinimide (NBS) and azobisisobutyronitrile (AIBN) to be able to quaternize the polymer afterward. Overall, the quaternization reaction generally proceeds via an S_N2 mechanism between a tertiary or secondary amine and an alkyl halide (as discussed in Papers II-IV), or with 1,4-butane sultone, as shown in Paper V.

The QA groups were synthesized based on tertiary amine and an alkyl halide, commonly known as a Menshutkin reaction. These reactions are typically performed in polar aprotic solvents like NMP or DMSO to ensure good solubility. Usually, no catalyst is needed; however, in some cases, like quinuclidone or N-methyl piperidone, adding K_2CO_3 helped full quaternization (**Scheme 6**). For introducing dual quaternary groups like bis-piperidinium, a low concentration of polymer solution was dropwise added to a solvent solution containing an excess of amine (up to 10 equiv.) to minimize crosslinking. A base is essential for facilitating the quaternization of secondary piperidines. Here, Hünig's base *N,N*-diisopropylethylamine (DIPEA), was used in some quaternization reactions, except those involving methyl iodide since it can react with DIPEA. For quaternization reactions of secondary amine with methyl iodide, K_2CO_3 was used.

The spirocyclic quaternization occurs in two key stages. The first stage, an intermolecular reaction, involves the reaction of a secondary amine with an α,ω -dibromoalkane to generate a tertiary amine. In the second stage, an intramolecular reaction occurs, and the newly formed tertiary amine reacts with an alkyl halide, resulting in the formation of the spirocyclic ring structure. A low concentration of polymer solution was added dropwise to the solution containing an excess of 1,5-dibromopentane to suppress crosslinking and favor intramolecular ring closure. Solvent selection, such as N-methyl-2-pyrrolidone (NMP) or dimethyl sulfoxide (DMSO), was based on polymer and product solubility.

Scheme 6. Quaternization of brominated benzylic positions (a), piperidine, and quinuclidine with alkyl halides (b and c) to form QA cations.



3.2 Characterization methods

3.2.1 Polymer characterization

Nuclear magnetic resonance spectroscopy (NMR)

The structure of all synthesized compounds was verified using NMR spectroscopy on a Bruker DRX 400 spectrometer. $\text{DMSO-}d_6$ ($\delta = 2.50$ ppm), CDCl_3 ($\delta = 7.26$ ppm), or D_2O ($\delta = 4.70$ ppm) was used as a solvent. In the former case, 5-10 vol% TFA was also added in order to shift the water peak downfield region; thus, the overlapped signals with the broad water signal in the upfield region ($\delta = 3.30$ ppm) were revealed. In addition, TFA protonates secondary or tertiary amines originating from degradation or incomplete quaternization reactions, which appear above 9 ppm. After alkaline treatment, the integration of the appeared amine peaks compared to the aromatic peaks of the polymer backbone, which were usually stable in alkaline media, can be used to calculate the ionic loss.

Size exclusion chromatography (SEC)

SEC was used to measure the number average molecular weight (M_n), weight average molecular weight (M_w), and polydispersity (Đ) of non-cationic polymers in Paper I. The mass distribution of precursor polymers was defined using the conventional calibration method. A calibration curve was attained through the elution time of standard samples with known molecular weight. Thus, the molecular weight of prepared samples was determined by comparing the elution time of the sample to the calibration curve. A Malvern Viscotek instrument equipped with two PL-Gel Mix-B LS columns (2×30 cm) and OmniSEC triple detectors (refractive index, viscosity, and light scattering) and chloroform was used as eluent at 35°C with a flow rate of 1 mL min^{-1} . For calibration, standard polystyrene (PS, $M_n = 96$ kDa, $\text{Đ} = 1.03$, Polymer Laboratories, Ltd.) was used. The samples were dissolved in the chloroform 24 h prior to measurements, and the polymer solutions were passed through a PTFE filter (pore size = $0.2\text{ }\mu\text{m}$) before running the measurements.

Intrinsic viscosity

Due to the limitations of the in-house SEC instruments, which use chloroform or tetrahydrofuran as eluents that are not proper solvents for the polymers in Papers II-V, the intrinsic viscosity ($[\eta]$) was measured as an indication of the molecular weight of polymers. This method relies on the fact that the dissolution of the polymer in the solvent will increase the viscosity of the final polymeric solution, which depends on different factors, including the type and molecular weight of polymers, concentration, temperature, and choice of solvent. In the case of ionic polymers, the degree of ionization and charge density are also important. Thus, a suitable amount of salt is added to avoid the polyelectrolyte effect. The measurements in this thesis were carried out using a Ubbelohde viscometer at 25 °C. The measurements were conducted in a water bath to maintain a constant temperature. First, the blank solution, 0.1 M LiBr in DMSO, was prepared, and the efflux time was recorded as t_b . The samples in bromide form were dried completely and then precisely weighed and dissolved in the blank solution with an initial concentration of 0.1 g dL⁻¹. Then, the efflux time of the solution was recorded, and the solution was diluted to several precise concentrations. The efflux time was recorded for more diluted solutions as t_s . Each concentration was measured four times, and the average was taken. The inherent (η_{inh}) and reduced (η_{red}) viscosities were calculated as:

$$\eta_{inh} = \frac{\ln\left(\frac{t_s}{t_b}\right)}{c} \quad (1),$$

$$\eta_{red} = \frac{\frac{t_s}{t_b} - 1}{c} \quad (2).$$

The intrinsic viscosity ($[\eta]$) was calculated by the intersections of the linear regressions of η_{inh} and η_{red} with the y -axis, zero polymer concentration ($c=0$).

Thermogravimetric analysis (TGA)

The thermal decomposition temperature of precursor polymers and membranes was studied in dry bromide form using TGA Q500 (TA instruments). All samples were first preheated up to 150 °C for 15 to 20 minutes to remove solvent residue before running the main cycle between 50 to 600 °C at a heating rate of 10 °C min⁻¹. The measurements were carried out under N₂ atmosphere. The weight changes were recorded giving TGA traces, and the decomposition temperature was noted at 5% weight loss ($T_{d,95}$).

Differential scanning calorimetry (DSC)

Differential scanning calorimetry (DSC) is a thermo-analytical technique used to investigate the response of polymer to heating. This technique was used to study the precursor polymers in Paper I. In DSC, the difference in heat flow is compared between the sample and the reference at the same temperature and is presented as a function of temperature. All the measurements were carried out under a N₂ atmosphere using Q2000 DSC (TA instruments). For each sample, a three-cycle heating-cooling-heating procedure was used. The first heating cycle was applied to eliminate the thermal history of the material, which may affect the final result. The glass transition temperature was taken as the inflection point in the thermogram during the second cycle.

3.2.2 Membrane preparation and characterization

Membrane Preparation

All quaternized polymers were cast in Petri dishes from 5% solutions of the respective polymer in DMSO or NMP at 80 °C. After drying, the membranes were detached from the dishes by adding deionized water and then stored in 1 M aq. NaBr 72 h to ion exchange to bromide form. Finally, the membranes were washed repeatedly to remove excess NaBr salt before being kept in deionized water for further characterization. The samples in hydroxide form were prepared by soaking them in 1 M aq. NaOH for 72 h, during which the alkaline solution was replaced at least three times. Then, the samples were washed with degassed deionized water quickly and repeatedly until the water remained neutral pH. The samples in hydroxide form were stored in degassed deionized water under N₂ atmosphere to prevent CO₂ contamination.

Ion exchange capacity (IEC)

The ion exchange capacity, defined as the number of charges in milliequivalent per gram of dry polymer, was calculated through the ¹H NMR spectroscopy as a theoretical value and through titration as an experimental value. The IECs of AEMs in bromide form were measured by Mohr titration. The samples in bromide form were completely dried and then precisely weighed before being immersed in 25 mL of 0.2 M aq. NaNO₃ and kept for at least 72 h at around 50 °C to ensure complete ion exchange. During this time, the vials were carefully sealed to avoid water evaporation. Subsequently, this solution was divided into 4 aliquots of 5 mL each. These aliquots were then titrated against 0.01 M aq. AgNO₃ using potassium chromate (K₂CrO₄) as an indicator. The average value of the endpoints from 4 titrations was used to calculate the IEC in the bromide and hydroxide form.

$$IEC_{OH} = \frac{IEC_{Br}}{1 - (0.0629 \times IEC_{Br})} \quad (3).$$

Water uptake and swelling ratios

The water uptake of the membranes at different temperatures between 20 and 80 °C was measured gravimetrically. Samples in bromide form were dried at 50 °C under vacuum for at least 48 h, and then the weight ($m_{\text{dry, Br}}$), thickness ($t_{\text{dry, Br}}$), and length ($l_{\text{dry, Br}}$) were measured carefully. Then, the samples were ion exchanged to hydroxide form as described above. Afterward, the samples were equilibrated in degassed deionized water at 20 °C for 24 h under N₂ and for 8 h at 40, 60, and 80 °C. The samples were taken out and wiped gently to remove the excess water on the surface, and the weight ($W_{\text{wet, OH}}$), length ($l_{\text{wet, OH}}$), and thickness ($t_{\text{wet, OH}}$) in the hydrated state were measured. The water uptake value was calculated as:

$$WU = \frac{W_{\text{wet, OH}} - W_{\text{dry, OH}}}{W_{\text{dry, OH}}} \times 100\% \quad (4)$$

while the swelling ratio values were calculated as:

$$SW_{\text{in-plane}} = \frac{l_{\text{wet, OH}} - l_{\text{dry, Br}}}{l_{\text{dry, Br}}} \times 100\% \quad (5),$$

$$SW_{\text{through-plane}} = \frac{t_{\text{wet, OH}} - t_{\text{dry, Br}}}{t_{\text{dry, Br}}} \times 100\% \quad (6).$$

Dynamic mechanical analyzer

A Dynamic Mechanical Analyzer (DMA) with tension clamps in force-controlled mode at a constant temperature was used to generate the stress-strain curve of membranes in Papers II, IV, and V (**Figure 8**). In this method, a controlled force was applied to the membrane while maintaining a fixed temperature, and the resulting strain was measured. The stress-strain curve provides essential information on the mechanical behavior of the membrane, including its Young's modulus, elongation at break, and ultimate tensile strength. This technique is crucial for assessing the mechanical properties of materials, such as stiffness, flexibility, and structural integrity, under defined thermal conditions.

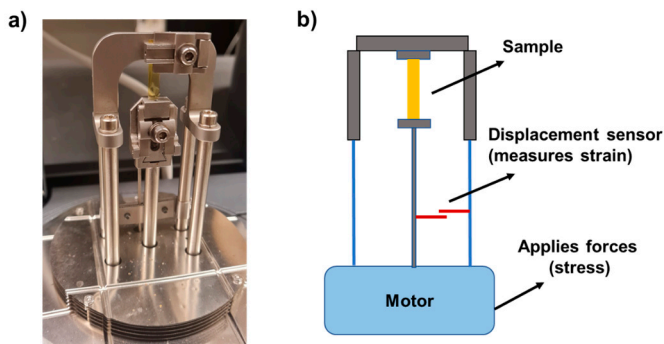


Figure 8. Photo of a sample in tension clamp in DMA (a), and the schematic of DMA (b).

Small angle X-ray scattering

The morphology of the dry samples in bromide form was studied by small angle X-ray scattering (SAXS). In SAXS, a collimated monochromatic X-ray beam illuminates the sample, and the elastic scattering at small angles is detected by a detector (**Figure 9**).

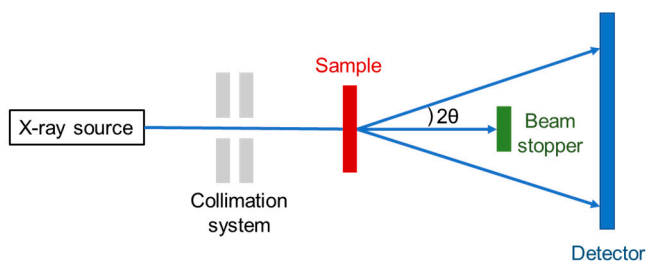


Figure 9. Schematic illustration of a SAXS experiment setup.

If the sample is phase-separated, the difference in electron density between phases shows as an angular distribution of the scattering. The intensity of the scattering is reported as a function of the scattering angle (2θ), which is used to define the scattering vector (q) using the following equation:

$$q = \frac{4\pi}{\lambda} \sin \theta \quad (7).$$

where λ is the wavelength of the X-rays. The microphase structure in AEMs is based on the incompatibility of the hydrophobic backbone and hydrophilic cations, which can be detected by SAXS as an intensity maximum known as "ionomer peak" (**Figure 10**).

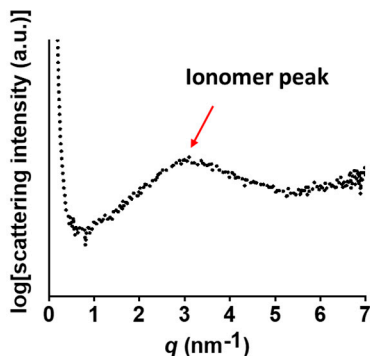


Figure 10. SAXS profile of an AEM with a clear phase separation.

The average distance between the ionic clusters, also known as the characteristic separation distance (d) is calculated from the q_{\max} and according to the Bragg's law:

$$d = \frac{2\pi}{q} \quad (8).$$

The characteristic separation distance calculated from SAXS results of AEMs is related to the distance between clusters and is affected by the molecular structures.

All the SAXS results presented in Paper I-III were measured using a SAXSLAB SAXS Instrument from JJ X-ray A/S, Denmark, in the q -ranges of 0.12-8 nm⁻¹ employing Cu K α radiation with a wavelength of $\lambda = 1.542$ Å. The results presented in Papers IV and V were carried out through a Xeuss 3.0 instrument (Xenocs, France) combined with Eiger2 R 1 M 2D-detector (Dectris). X-ray source was producing a photon beam with a wavelength of $\lambda = 1.34$ Å.

Atomic force microscopy (AFM)

The AFM images recorded in Papers II, IV, and V were obtained using a Bruker Icon Atomic Force microscope instrument. Tapping mode analysis of the air facing side of the membrane was performed, scanning 1 $\mu\text{m} \times 1 \mu\text{m}$ areas at a scan rate of 0.498 Hz.

Ion conductivity

Ion conductivity of samples in the fully hydrated state was measured between 20-80 °C by electrochemical impedance spectroscopy (EIS), using a NovoControl high-resolution dielectric analyzer V 1.01 S. The in-plane resistance of samples was measured using an AC voltage with an amplitude of 50 mV at 10⁰-10⁷ Hz. In order to measure the in-plane resistance (R), the sample was quickly assembled into a 2-probe cell, as shown in **Figure 11**, in a way that the two stainless steel electrodes

were placed alongside opposite edges of the sample. The compact assembly was placed in a Teflon holder, and degassed deionized water was added to keep the sample hydrated. Subsequently, the cell was sealed with brass plates and plastic screws.

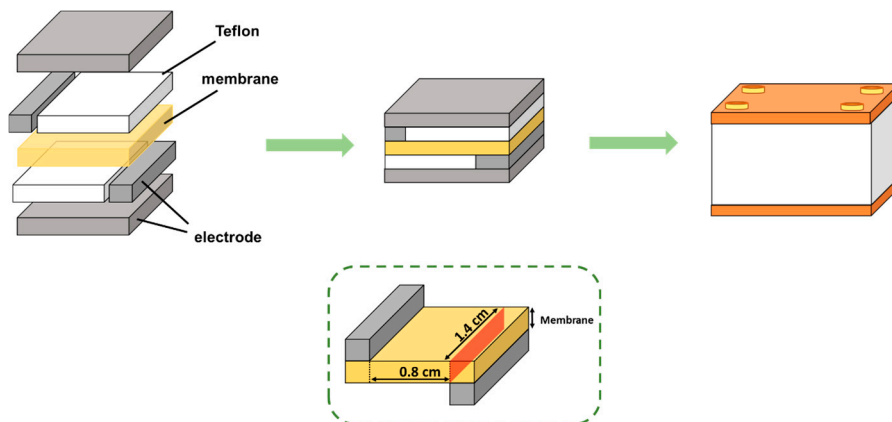


Figure 11: Sample cell configuration for EIS experiment.

From the measured R values at different frequencies, the conductivity of the sample (σ) was calculated by the device according to the following equation:

$$\sigma = \frac{L}{R \times A} \quad (9).$$

where L is the distance between two rectangular electrodes, which is 0.8 cm, and A is the area of the effective cross-section of the membrane. The acquired conductivity data from the instrument was plotted as a function of frequency, and the plateau value was reported (**Figure 12**). For each AEM, at least two samples were measured.

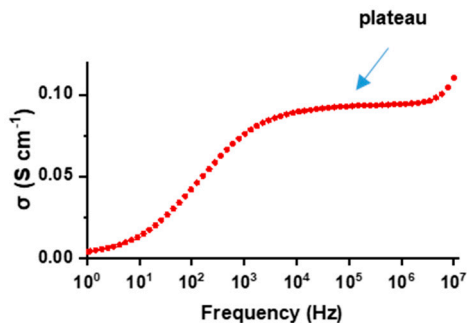


Figure 12. Hydroxide conductivity data of AEM as a function of frequency at a constant temperature.

Chemical stability

In order to assess the chemical resistance of an AEM in alkaline media, the samples were treated in aq. NaOH solutions at elevated temperatures and their chemical structure were studied using NMR analysis to determine the degradation mechanism and calculate the degree of degradation, specifically by ionic loss. Initially, samples were aged at 80 °C, since it is a prevailing operation temperature for many fuel and electrolyzer cells.¹²⁶ In order to accelerate the degradation reactions for ease of illuminating the active degradation mechanisms, in many cases, the temperature was raised to 90 °C. Furthermore, it was found that the molarity of the alkaline solution has a significant role in the degradation rate. Throughout the thesis, the concentration of alkaline solution was varied between 1-10 M. The alkaline treatment was carried out in a sealed pressure-resistant glass tube containing a Teflon insert to prevent water evaporation and maintain the temperature and concentration constant during the experiment (**Figure 13**).

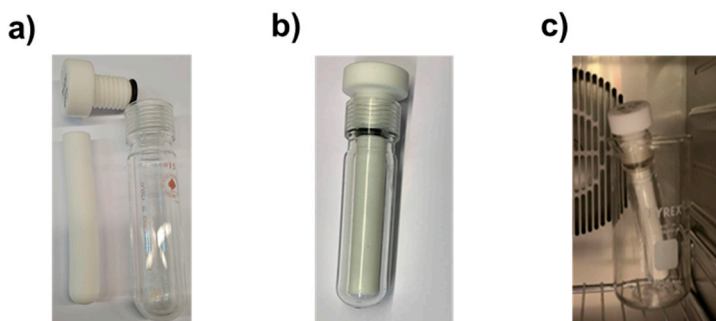


Figure 13. Assembled sample holder containing a thick pressure sustainable glass tube with a Teflon inner tube and a screw (a), the assembled holder (b), and the set up placed in a ventilated oven (c).

After different intervals, the samples were taken out and washed with deionized water. Then, the samples were ion-exchanged to bromide form, thoroughly washed with deionized water, and dried at room temperature under vacuum. Subsequently, the samples were dissolved in DMSO- d_6 with a small amount of TFA to shift the residual water signal and protonate any tertiary amine resulting from degradation, assisting the elucidation of the extent and mechanism of degradation. NMR spectroscopy was used to evaluate the alkaline stability of the AEMs in this thesis because it does not require much material, and it is easy to detect even low degrees of degradation with high accuracy. Furthermore, this technique helps to study the mechanism of degradation. The degree of degradation by specific degradation was estimated by comparing the signal intensity of each degradation product with the untreated sample. With the exception of Paper II, in all papers, the thermal stability of samples after alkaline treatments was studied by TGA as well.

4 Summary of appended papers

This chapter summarizes the results and findings of the synthesized AEMs via polyhydroxyalkylations included in this thesis. The chapter is divided into five parts, each representing one article. Each part explains the motivation for polymeric structure and a part of the properties of the corresponding AEMs.

4.1 Paper I: Poly(arylene alkylene)s with pendant benzyl-tethered ammonium cations

There has been a discussion about the stability of the N-alicyclic QA cations structure and ammonium groups placed at the benzylic group. An earlier study found that DMP and ASU possess significantly higher stability in 6 M aq. NaOH solution at 160 °C.¹¹⁵ However, according to Dekel and co-workers, benzyl trimethylammonium (BTMA) compounds may remain more stable at very low hydration levels compared to ASU during AEMFC operation at the cathode.^{113, 115} A previous work described that at low microsolvation levels, the basicity of hydroxide ions is more affected by the hydration level than its nucleophilicity, which explains why the BTMA is more stable than ASU at lower hydration conditions.¹¹²

All the studies mentioned above were conducted on the molecular compounds and not on the polymeric structure, which motivated us to design a project to investigate how placing different QA groups at the benzylic position in the polymer structure affects the overall stability of AEMs. For this purpose, we synthesized two ether-free poly(arylene alkylene)s based on *p*-terphenyl and biphenyl, respectively, *via* superacid-mediated Friedel–Crafts. Then, the benzylic positions were brominated and subsequently utilized for incorporating various mono- and di-QAs via Menshutkin reactions (**Scheme 7**). The IEC of the final AEMs was controlled by adjusting the degree of bromination of corresponding precursor polymers. The resulting quaternized compounds were denoted as PT-QA-*y* and PB-QA-*y*, where QA denotes the cation and *y* is the ion exchange capacity (IEC, mequiv g⁻¹) value of the sample in the hydroxide form, as determined *via* Mohr titration. In general, the samples functionalized with alicyclic QAs displayed higher thermal stability. For instance, the decomposition temperature for PB-TMA-2.1 was 227 °C, while for PB-Qui-1.8, and PB-bisPip-2.2 was 255 and 299 °C.

Scheme 7. Synthetic pathways to PT and PB functionalized with mono- and di-QA groups, respectively.

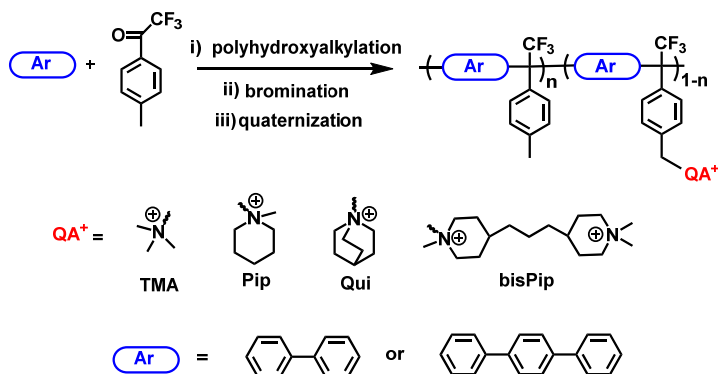


Table 1. Properties of AEMs

Sample	IEC ^a (mequiv.g ⁻¹)	WU _{OH, 80 °C} ^b (wt%)	λ _{OH, 80 °C} ^b	σ _{OH, 80 °C} ^b (mS cm ⁻¹)	T _{d, 95} ^c (°C)
PT-TMA-1.7	1.57 (1.74)	61	19	41	206
PT-Pip-1.6	1.48 (1.64)	57	19	29	225
PT-bisPip-2.15	1.90 (2.15)	104	27	113	257
PT-bisPip-2.35	2.04 (2.35)	155	36	133	256
PB-TMA-2.1	1.91 (2.11)	83	22	69	227
PB-Pip-2.0	1.80 (2.03)	79	21	66	228
PB-Qui-1.8	1.67 (1.80)	69	19	53	299
PB-bisPip-2.2	1.93 (2.19)	153	38	93	255
PB-bisPip-2.4	2.09 (2.40)	203	46	81	281
PB-bisPip-2.6	2.24 (2.60)	NA ^d	NA ^d	NA ^d	246

^a Calculated from IEC_{Br} values obtained by titration (values in hydroxide form within parentheses), ^b Measured at 80 °C under fully hydrated conditions (immersed), ^c Measured by TGA under N₂ at 10 °C min⁻¹, ^d AEM was very brittle and was not analyzed.

The mono-QA functionalized membranes in hydroxide form showed a moderate water uptake; however, after tethering the di-cationic bisPip groups, the water uptake increased dramatically because of the higher IEC values. The same trend was also observed in hydroxide conductivity. For example, PB-TMA-2.1 showed 69 mS cm⁻¹ hydroxide conductivity with 83% water uptake at 80 °C, while PB-bisPip-2.2, with a similar IEC value, reached 93 mS cm⁻¹ with corresponding 153% water uptake. The comparison of conductivity and water uptake at 80 °C as a function of IEC is given in **Figure 14**.

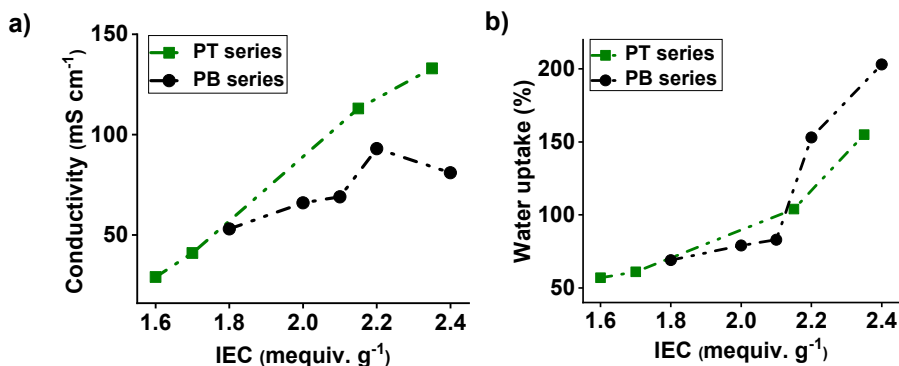


Figure 14. Hydroxide conductivity and water uptake of AEMs in PT and PB series at 80 °C as a function of IEC.

There are various pathways through which AEMs may degrade in an alkaline environment, leading to the loss of cations and ultimately decreasing the IEC and conductivity. ^1H NMR spectroscopy was used to investigate any structural changes after the alkaline treatment of the AEMs in 1, 5, and 10 M of aq. NaOH, respectively, at 80 °C. The spectra of samples after storage in 1 M aq. NaOH for 168 and 504 h for two samples is given in **Figure 15**. After different storage times, the samples were taken out, ion-exchanged to the bromide form, dried, and dissolved in a mixture of $\text{DMSO-}d_6$ and TFA before ^1H NMR analysis.

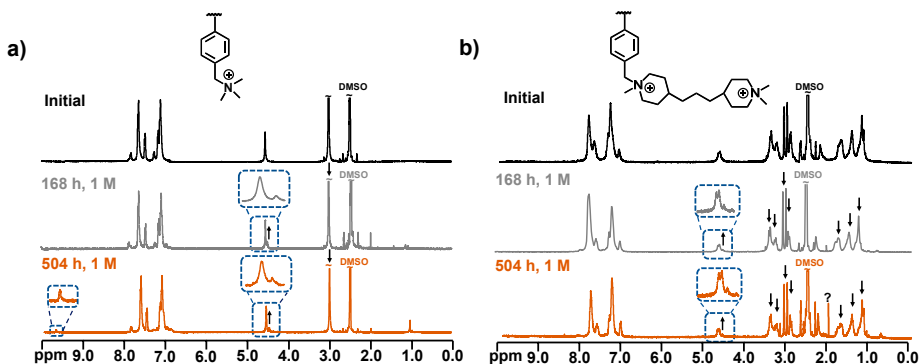


Figure 15. ^1H NMR spectra of PB-TMA-2.1 (a), PB-bisPip-2.2 (b) before and after storage in 1 M aq. NaOH at 80 °C.

At all investigated conditions, nucleophilic substitution at the benzylic position was the main degradation pathway; however, increasing the alkali concentration triggered additional degradation pathways, such as ring-opening and methyl

substitution reactions. The results showed that the benzylic position is highly susceptible to nucleophilic substitution (**Figure 16**). In addition, a correlation between the QA structure and the total ionic loss was found. The bulkier cation, Qui, showed a lower degree of degradation, probably due to the partial steric shielding of benzylic positions and the cage-shaped structure.

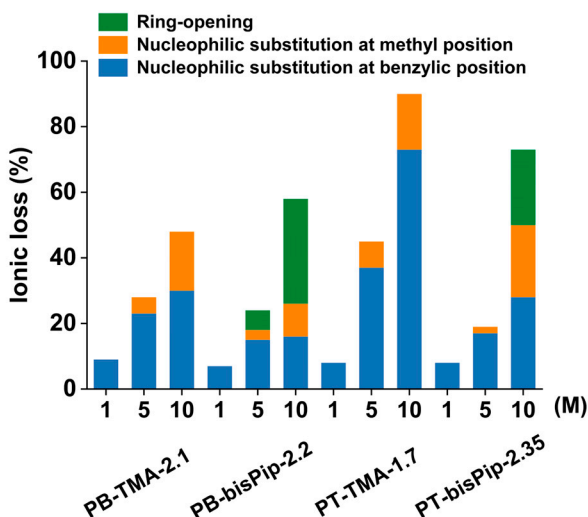


Figure 16: Ionic loss of the AEMs after storage in 1, 5, and 10 M aq. NaOH at 80 °C for 168 h.

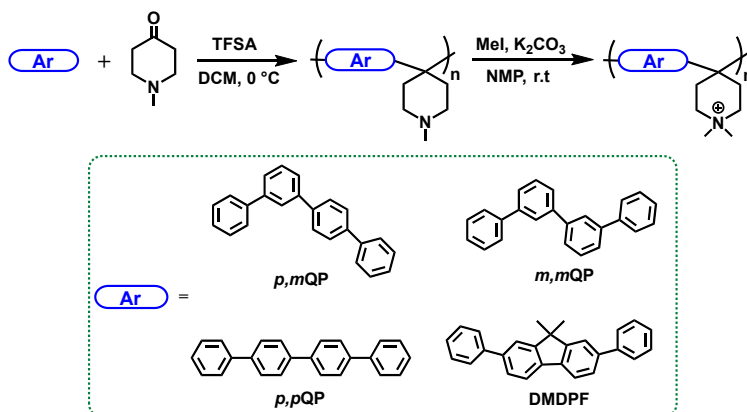
4.2 Paper II: Tuning the properties of AEMs by changing the configuration of arene

In Paper II, we investigated the influence of monomer configuration on the final structure and the properties of the regarded membranes. Ether- and fluorine-free hydroxide-conducting poly(quaterphenyl piperidinium) membranes with relatively high and comparable IECs around 2 mequiv. g⁻¹ were synthesized using three isomers of quaterphenyl monomer with different configurations, *p,p*-, *p,m*-, and *m,m*QP. Using quaterphenyl isomers enabled us to have a moderate IEC value without needing to copolymerize with a co-monomer like TFAP, which has been commonly used to regulate the IEC of poly(arylene piperidinium)s.^{97, 155, 156} Furthermore, as the flexibility of the monomer changes, it provides the opportunity to tune the flexibility and conformation of the backbone, thereby influencing the properties of AEMs.

For this purpose, *p,m*-, and *m,m*QP, were synthesized through Suzuki coupling, and together with the commercially available *p,p*QP were implemented in super acid-catalyzed polyhydroxyalkylation to prepare a series of homopolymers (**Scheme 8**).

Since the molecular formulas of the repeating units are identical, the IECs for all the samples are the same, and the properties can be mainly attributed to the difference in the configuration of polymer structures and molecular weight. We have also investigated the possibilities of preparing copolymers containing two different quaterphenyl isomers. Furthermore, the results were compared with the PDPF-Pip due to the similarity between the DMDPF structure and quaterphenyl, which makes it quite a rigid compound with a rigidity between *p,p*QP, and *p,m*QP.

Scheme 8. Synthetic pathway towards *x,x*-QuPip, and PDPF-Pip in Paper II.



All AEMs showed high thermal stability with $T_{d,95}$ of 256 °C or higher. Furthermore, the intrinsic viscosity values were measured for quaternized samples dissolved in 0.1 M LiBr in DMSO at 25 °C, and the $[\eta]$ values were in the range between 0.38 and 0.76 dL g⁻¹ (Table 2).

Table 2. Properties of AEMs

AEM	IEC ^a (mequiv. g ⁻¹)	WU _{OH,80 °C} ^b (wt%)	$\sigma_{OH,80 °C}$ ^b (mS cm ⁻¹)	$\lambda_{OH,80 °C}$ ^b	$T_{d,95}$ ^c (°C)	$[\eta]$ ^d (dL. g ⁻¹)
<i>m,m</i> -QuPip	2.03 (2.32)	209	178	50	305	0.41
<i>p,m</i> -QuPip	2.04 (2.34)	145	156	34	273	0.76
<i>p,p</i> -QuPip	2.03 (2.32)	37	96	9	276	0.54
<i>co</i> -QuPip	2.01 (2.30)	116	142	28	256	0.50
PDPF-Pip	1.89 (2.14)	104	124	27	318	0.38

^a Calculated from IEC_B, values obtained by titration (values in hydroxide form within parentheses), ^b Measured at 80 °C under fully hydrated conditions (immersed), ^c Measured by TGA under N₂ at 10 °C min⁻¹, ^d evaluated from extrapolating η_{red} and η_{inh} to $c = 0$.

As shown in **Figure 17**, the data of hydroxide ion conductivity and water uptake of fully hydrated membranes at 80 °C revealed the impact of structure variation on the properties. For instance, at 80 °C, *m,m*-QuPip showed water uptake and hydroxide conductivity of 209% and 178 mS cm⁻¹, respectively, while *p,p*-QuPip displayed 37% water uptake and 96 mS cm⁻¹ hydroxide conductivity. The other samples, *p,m*-QuPip, and PDPF-Pip, displayed 156 and 124 mS cm⁻¹, with corresponding water uptake of 145% and 104%, respectively, at 80 °C. A possible explanation why *m,m*-QuPip, and *p,m*-QuPip had significantly higher hydroxide ion conductivity and water uptake values compared to *p,p*-QuPip is due to the flexibility of their structures.

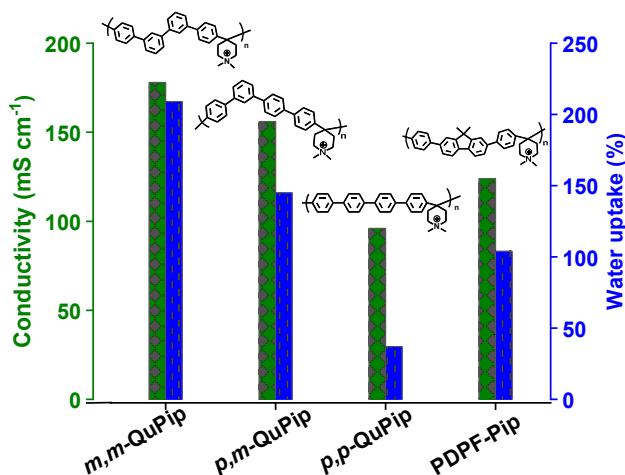


Figure 17. Hydroxide conductivity and water uptake of AEMs in a fully hydrated state at 80 °C.

The results of alkaline stability in 1, and 2 M aq. NaOH at 80 and 90 °C and time intervals were investigated and summarized in **Figure 18**. Based on polymer structure, the primary degradation pathway is through ring opening by Hofmann β -elimination. After storage of samples in 1 M aq. NaOH at 80 °C for 360 h, only very small and barely detectable signals from degradation products were recorded, while after 720 h, traces of degradation were increased, with *p,p*-QuPip showing the highest degradation. After treating the samples in harsher conditions of 2 M aq. NaOH at 90 °C, the rate of degradation increased, and all the samples displayed signs of degradation after 360 h. After 720 h, all samples also showed degradation through nucleophilic methyl substitution. *m,m*-QuPip had the highest alkaline stability with 8% total ionic loss, while PDPF-Pip showed the lowest stability with 19%. To gather further insights, the samples were subjected to the same alkaline conditions for 2400 hours. After this period, all AEMs experienced significant ionic loss, roughly double that observed after 720 hours, with Hofmann ring-opening β -elimination remaining the predominant degradation mechanism.

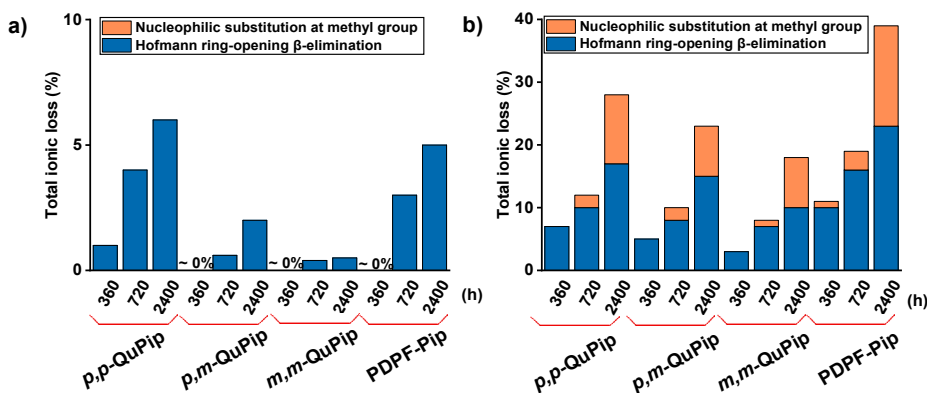


Figure 18. Ionic loss of the AEMs after storage in 1 M aq. NaOH at 80 °C (a) and 2 M aq. NaOH at 90 °C.

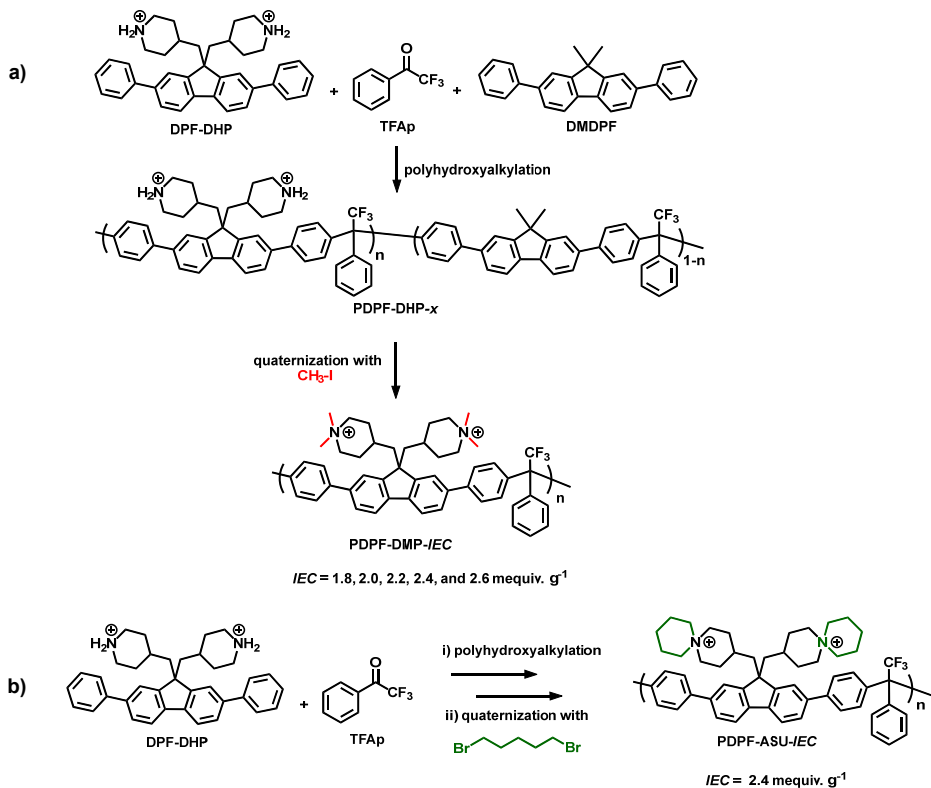
4.3 Paper III: The effect of alkyl spacers in the alicyclic QA

Fluorene-based monomers were chosen as the electron-rich arene domain in this work. Fluorene is an *ortho*-fused tricyclic structure with a rigid planar structure, which has two six-membered benzene rings attached to either side of a five-membered ring. Furthermore, the two weakly acidic protons in the five-membered ring are highly reactive in the presence of a base and can be used for modification through S_N2 alkylation. Diphenylfluorene monomer derivatives possess a more rigid structure than their non-phenylated counterparts, facilitating the polyhydroxyalkylation reaction and enabling the construction of polymers with higher chain rigidity, which in turn reduces water uptake and swelling in AEMs.

The polymer architectures described in Paper III feature a novel molecular structure of fluorene-based monomer tethered with piperidinium-based cations attached at the 4-position, demonstrating high alkaline stability. In previous work in our group, a long and flexible seven-carbon alkyl chain was used to tether the cation group to the polymer backbone.^{99, 150} It has been reported that alkyl chains with 4-6 carbons enhance phase separation, promote the formation of ionic clusters and percolation channels, and facilitate fast ion transport. However, longer alkyl chains (>6 carbons) negatively affect the alkaline stability of the cationic group and reduce the glass transition temperature of the polymers, resulting in a softer material. Additionally, introducing long alkyl chains in the fluorene-based monomer increases the molecular weight of the repeating unit, thereby sacrificing the total ion exchange capacity (IEC).¹⁵⁰ In this work, piperidinium-based cations are attached at the 4-position on a diphenylated fluorene monomer via an alkylation reaction. Using methyl bridges instead of the seven-carbon alkyl chain to tether the cationic group reduces the molecular weight of the functionalized repeating unit, enabling better control of the final IEC. Synthesized di-cationic monomer DPF-DHP, and non-ionic

DMDPF were polymerized via a superacid-catalyzed polycondensation reaction using TFAP as a ketone to produce the precursor PDPF-DHP-*x* series, where *x* represents the mole percentage of the ionic unit in the copolymers (**Scheme 9**). The precursor polymers were then quaternized with methyl iodide and 1,5-dibromopentane to create the PDPF-DMP-*IEC* and PDPF-ASU-*IEC* series, respectively. The effect of the methyl bridge was investigated in terms of morphology, water uptake, thermal and alkaline stability, and ionic conductivity and compared with previously published work.

Scheme 9. Synthetic routes and structures of cationic polymers in Paper III.



SAXS measurements revealed that introducing piperidinium-based cations via a methyl bridge promotes phase separation in AEMs, resulting in distinct ionomer peaks (**Figure 19a**). For the PDPF-DMP-*IEC* series, the characteristic distance (*d*) decreased as the IEC value increased. Additionally, the structure of the cationic group also influenced the characteristic distance; for example, at similar IEC values, PDPF-DMP-2.4 and PDPF-ASU-2.4 exhibited *d* values of 2.25 nm and 1.91 nm, respectively. The presence of phase separation and ionic clustering formed a percolating channel, leading to higher ionic conductivities.

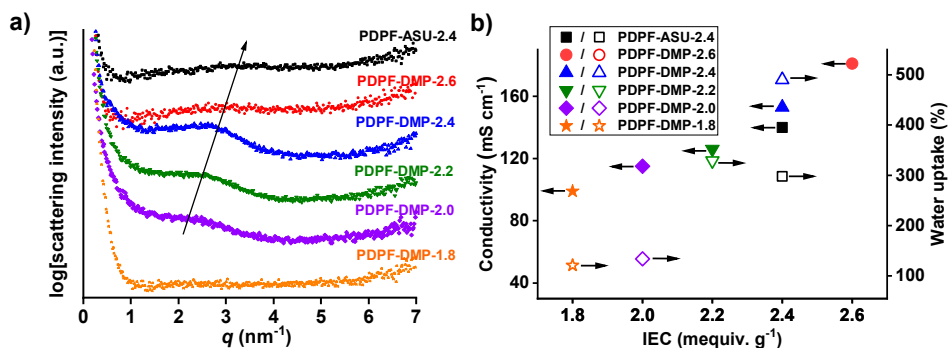


Figure 19. SAXS profile of PDPF-DMP-IEC series and PDPF-ASU-IEC (a) and hydroxide conductivity and water uptake of samples at 80 °C in a fully hydrated form as a function of IEC.

The water uptake and hydroxide conductivities of the AEMs were measured, with the results presented in **Table 3** and **Figure 19b**.

Table 3. Properties of AEMs

AEM	IEC ^a (mequiv. g ⁻¹)	WU _{OH,80 °C} ^b (wt%)	$\lambda_{OH,80 °C}$ ^b	σ_{OH} ^b (mS cm ⁻¹)	$T_{d,95}$ ^c (°C)	[PRE] ^d (dL. g ⁻¹)
PDPF-DMP-1.8	1.61 (1.80)	121	36	99	269	0.67
PDPF-DMP-2.0	1.83 (2.06)	134	36	115	246	0.69
PDPF-DMP-2.2	1.93 (2.18)	290	84	126	283	0.79
PDPF-DMP-2.4	2.13 (2.46)	490	111	153	282	0.85
PDPF-DMP-2.6	2.23 (2.59)	NA	NA	181	310	0.81
PDPF-ASU-2.4	2.10 (2.41)	298	64	140	335	0.81

^a Calculated from IEC_{Br} values obtained by titration (values in hydroxide form within parentheses), ^b Measured at 80 °C in the OH⁻ form in the fully hydrated state, ^c Measured by TGA at 10 °C min⁻¹ under N₂, ^d evaluated from extrapolating η_{red} and η_{inh} to c = 0.

Water uptake and hydroxide conductivity showed an explicit dependency on the IEC across all AEMs. At 80 °C, PDPF-DMP-1.8 exhibited 3.4 times lower water uptake than that of PDPF-DMP-2.4 with corresponding 99 and 153 mS cm⁻¹ hydroxide conductivity, respectively (**Figure 19b**). PDPF-DMP-2.4 showed water uptake of 490% with hydroxide conductivity of 153 mS cm⁻¹ at 80 °C and PDPF-ASU-2.4 with similar IEC value displayed 298% water uptake with 140 mS cm⁻¹ at 80 °C. The lower water uptake of PDPF-ASU-2.4 can be attributed to the bulkier and less hydrophilic structure of the ASU group and lower water uptake. The hydroxide conductivity of PDPF-DMP-2.6 was nearly double that of PDPF-DMP-1.8.

The alkaline stability of the PDPF-DMP-IEC series and PDPF-ASU-IEC was assessed using ^1H NMR spectroscopy. The AEMs were stored in 2 M aq. NaOH for 30 days and in 5, 7, and 10 M aq. NaOH at 90 °C for 168 hours. Comparing the changes in the ^1H NMR spectra of the AEMs before and after alkaline treatment allowed us to determine the degradation mechanisms pathway and quantitatively calculate the ionic loss. All AEMs demonstrated high alkaline stability, showing no degradation after 720 h in 2 M aq. NaOH and 168 hours in 5 M aq. NaOH at 90 °C. However, at the harsher condition, 10 M aq. NaOH at 90 °C for 168 h, the samples showed degradation. ^1H NMR spectra of PDPF-DMP-2.2 is given as an example (**Figure 20a**). No changes were observed in the aromatic region in the ^1H NMR spectrum, indicating a high alkaline stability of the backbone. The ionic loss was calculated by comparing the integration of newly emerged signals to that of the entire aromatic region. The new proton signals at ~ 4.0 ppm (*c*), 4.2 (*c*) ppm, and ~ 5.0 (*d*) ppm showed an integration ratio of 1:1:1, correlating with the formation of vinylic protons, most probably through Hofmann elimination. Moreover, the corresponding tertiary amine proton formed in Hofmann elimination gave a signal at 9.12 (*a*) ppm. The new and small signal at ~ 8.9 (*a'*) ppm was correlated to the tertiary amines formed by nucleophilic substitution. Hofmann elimination was the dominant degradation pathway, which decreased with increasing IEC values. Among all the samples, PDPF-DMP-2.6 showed the highest alkaline stability with 27% total ionic loss.

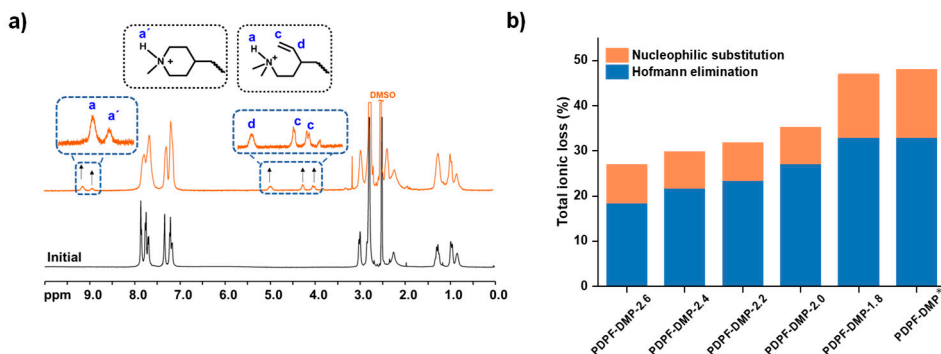


Figure 20. Alkaline stability of the PDPF-DMP-2.2 membrane after 168 h storage in 10 M aq. NaOH at 90°C (a), and total ionic loss of the PDPF-DMP-IEC series and PDPF-DMP¹⁵⁷ after alkaline treatment in 10 M, aq. NaOH for 168 h at 90°C (b).

All the presented AEMs showed lower total ionic loss than PDPF-DMP, where the piperidine-based cation group was attached via a seven-carbon alkyl spacer (**Figure 20b**).¹⁵⁷ Additionally, the number of water molecules per hydroxide ion (i.e., the λ -value) may play a role in enhancing the alkaline stability of the current AEMs, as higher hydration levels reduce the reactivity of hydroxide ions. PDPF-ASU-IEC

could not be dissolved in DMSO- d_6 and analyzed after immersion in 10 M aq. NaOH for 168 h at 90 °C.

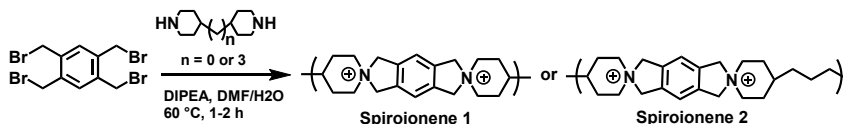
To conclude, introducing the alicyclic piperidine-based cationic group via a methyl bridge to the polymer backbone can be considered a new and efficient strategy to improve the properties of AEMs.

4.4 Paper IV: *N*-Spirocyclic quaternary ammonium ionene

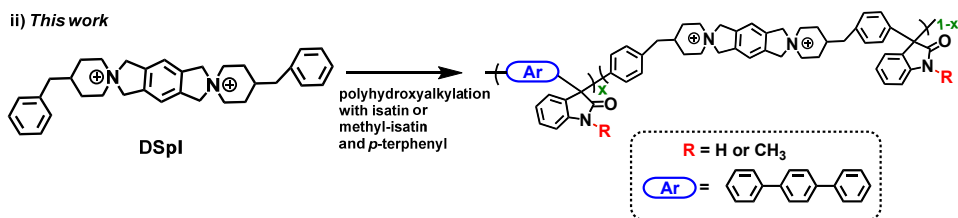
Previously in our group, aryl ether-free spiro-ionenes were synthesized through cyclo-polycondensation as potential anion conducting polymers to overcome low alkaline stability issues (**Scheme 10**).¹⁰² These materials displayed high thermal stability with high IEC values. Both ionenes were stable at 1 M KOD/D₂O at 80 °C for 672 h, and Spiroionene 2 did not degrade even after storage for 1896 h. However, they were soluble in water, necessitating blending with PBI-OO to make water-insoluble membranes. After blending, the samples showed high hydroxide conductivity, up to 120 mS cm⁻¹ at 80 °C for S70P30. These were in agreement with the other work that reported high stability for the model compound of P-ASN.¹⁵⁸

Scheme 10. Synthetic routes towards Spiroionenes¹⁰² and the series of Splsx in Paper IV.

i) *Previous work*



ii) *This work*



All the mentioned results motivated us to separate the spiro-centered QA cation along the ionene to reduce the IEC and water uptake while retaining their alkaline stability without the need to blend. For this purpose, a dispirocyclic QA monomer, DSpl, was synthesized by using the commercially available 1,2,4,5-tetrakis(bromomethyl)benzene (4BMB) and 4-benzyl piperidine. The synthesized monomer was reactive enough to polymerize in Friedel-Crafts type polycondensation with isatin as a ketone. The homopolymer gave a high IEC of 3.02 mequiv g⁻¹ in the hydroxide form; thus, for lowering the IEC values, *p*-terphenyl was used as a comonomer in the polymerization reaction to gain a series of

copolymers with lower IEC values. Li et al. reported that methylated isatin can lead to lower alkali absorption, leading to higher alkaline stability of the polymer by closely retaining IEC values.¹¹⁸ Therefore, two copolymers were synthesized by implementing commercially available methyl isatin in polymerization to investigate further the effect of N-modified isatin on the properties of the membranes.

Table 4. Properties of AEMs

AEM	IEC ^a (mequiv.g ⁻¹)	WU _{OH,80 °C} ^b (wt%)	$\sigma_{\text{OH},80\text{ °C}}$ ^b (mS cm ⁻¹)	$\lambda_{\text{OH},80\text{ °C}}$ ^b	$T_{\text{d},95}$ ^c (°C)	$[\eta]$ ^d (dL. g ⁻¹)
SpIs100	2.57 (3.06)	282	152	52	346	0.30
SpIs60	1.93 (2.21)	148	136	35	351	0.34
SpIs50	1.75 (1.96)	92	86	26	338	0.32
SpIs40	1.50 (1.65)	41	56	14	342	0.43
SpMIs60	1.91 (2.17)	128	116	33	393	0.26
SpMIs50	1.70 (1.90)	112	103	33	383	0.24

^a Calculated from IEC_{Br} values obtained by titration (values in hydroxide form within parentheses), ^b Measured at 80 °C under fully hydrated conditions (immersed), ^c Measured by TGA under N₂ at 10 °C min⁻¹, ^d evaluated from extrapolating η_{red} and η_{inh} to $c = 0$.

The samples demonstrated high conductivity in both hydroxide and bromide forms. SpIs100 displayed a hydroxide conductivity of 152 mS cm⁻¹ with high water uptake of 282% at 80 °C, while with lowering IEC to 1.65 mequiv. g⁻¹ in SpIs40 the hydroxide conductivity reduced to 56 mS cm⁻¹ at the same temperature with 41% water uptake. The same trend was observed in bromide conductivity, where SpIs100 displayed the highest conductivity of 53 mS cm⁻¹, and the value was reduced by decreasing the IEC in copolymers (**Figure 21**).

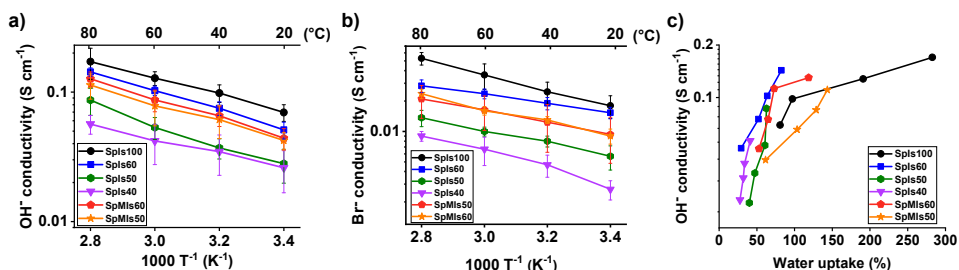


Figure 21. Hydroxide and bromide conductivity as a function of T^{-1} (a, b), and hydroxide conductivity as a function of water uptake.

The ring system contributed to high thermal stability, with all samples displaying decomposition temperatures ($T_{d,95}$) above 338 °C. In alkaline stability tests at 1 M aq. NaOH at 80 °C, the samples exhibited high stability with barely detectable signs of degradation in ^1H NMR; however, their stability decreased in 2 M NaOH at 90 °C. Among the three tested samples, SpIs100 had the highest stability with only 3% total ionic loss, while SpIs60 had 7%, and SpMIs60 showed the lowest stability with 17% ionic loss. Since TGA has a high sensitivity to any changes in the structure of the main backbone and ionic content, it was used to further investigate the alkaline stability of the samples after an alkaline stability test in 1 and 2 M aq. NaOH at 80 and 90 °C, respectively. As shown in **Figure 22**, TGA traces of SpIs100 after alkaline treatments roughly coincided well with the pristine sample.

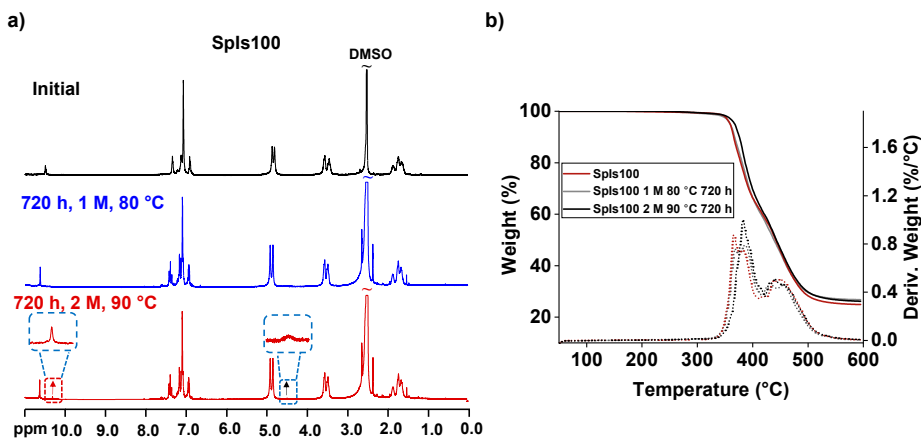
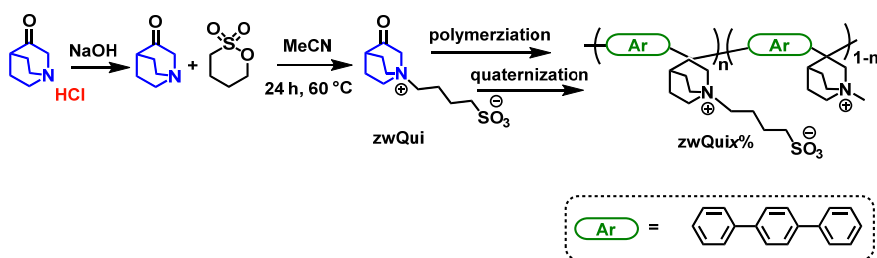


Figure 22. ^1H NMR spectra of SpIs100 in 1 and 2 M aq. NaOH at 80 and 90 °C, respectively, for 720 h (a), and TGA traces of samples before and after alkaline treatment in 1 and 2 M aq. NaOH at 80 and 90 °C for 720 h.

4.5 Paper V: zwitterionic poly(terphenylene quinuclidinium)

The molecular design and synthesis of zwitterionic polymers, which feature both cationic and anionic groups in the same side chain, represent a promising approach for enhancing the overall properties of IEMs.^{154, 159-161} These polymers offer a platform that combines the benefits of both PEMs and AEMs, leading to increasing interest in their application across various fields.^{160, 161} Typically, the high ionic content of zwitterionic polymers results in excellent ionic conductivity, while ionic crosslinking, facilitated by electrostatic interactions between the cationic and anionic groups, helps control water uptake.^{161, 162} Building on our previous work with zwitterionic poly(terphenyl piperidinium)s, which demonstrated high alkaline stability in 1 M aq. NaOH at 80 °C, we synthesized a zwitterionic monomer based on quinuclidinium, zwQui (**Scheme11**).¹⁵⁴

Scheme 11. Synthetic routes towards zwQui and zwQuix% in Paper V.



This monomer was directly used in polymerization with varying ratios of zwQui and 3-quinuclidinone hydrochloride to adjust the ionic content. The resulting polymers were fully quaternized through methylation of the tertiary amine. The quaternized copolymers were then cast into membranes, and their properties, incorporating both cationic and zwitterionic groups, were evaluated and compared to those from our earlier project.¹⁵⁴ The properties of the samples are given in **Table 5**.

Table 5. Properties of AEMs

AEM	IEC ^a (mequiv. g ⁻¹)	WU _{OH} ^b (wt%)	σ_{OH} ^b (mS cm ⁻¹)	$\lambda_{\text{OH}, 80\text{ }^\circ\text{C}}$ ^b	$T_{\text{d}, 95}$ ^c (°C)	$[\eta]^d$ (dL. g ⁻¹)
zwQui10%	2.12 (2.45)	143	139	32	350	0.35
zwQui30%	1.95 (2.23)	118	108	29	367	0.31
zwQui40%	1.83 (2.08)	94	100	25	373	0.45

^a Calculated from IEC_{Br} values obtained by titration (hydroxide form within parentheses), ^b measured at 80 °C under fully hydrated conditions (immersed), ^c measured by TGA under N₂ at 10 °C min⁻¹, ^d evaluated from extrapolating η_{red} and η_{inh} to $c = 0$.

These samples demonstrated an ion exchange capacity of 2.08 to 2.45 mequiv. g⁻¹ in hydroxide form, achieving high conductivity (100 to 139 mS cm⁻¹) and water uptake ranging from 94% to 143% at 80 °C (**Figure 23**). As the zwitterionic content increased, the water uptake and conductivity decreased, probably as a result of decreasing IEC and increasing ionic crosslinking.

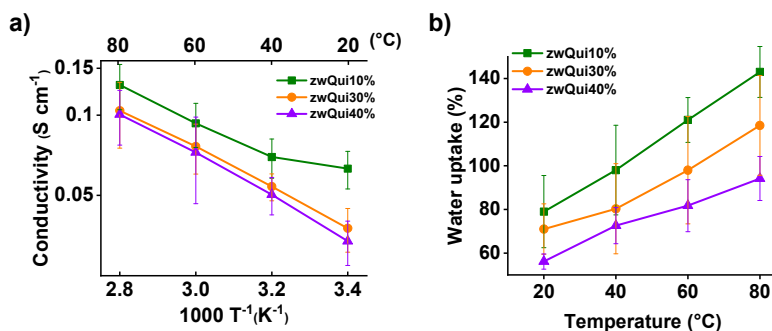


Figure 23. Hydroxide conductivity (a), and water uptake (b) as a function of T^{-1} and temperature, respectively.

All samples showed no sign of degradation at 2 M aq. NaOH at 90 °C (**Figure 24**). For further investigation, the samples were placed at 5 M aq. NaOH at 90 °C for 168 h, and they showed high stability with no detectable sign of degradation. Thus, the samples were tested in harsher conditions at 10 M aq. NaOH at 90 °C for 168 h, and they started to show degradation through nucleophilic substitution at the alkyl group. The alkaline stability of PTPzw30Q was also investigated in the same conditions as zwQui $x\%$, and it was revealed that the latter has much lower alkaline stability. For instance, PTPzw30Q showed 63% degradation through Hofmann elimination and 11% through nucleophilic substitution; however, zwQui30% showed 4% degradation through nucleophilic substitution. These results show high alkaline stability for zwQui $x\%$ samples, likely attributed to the cage-like structure of the bicyclic quinuclidinium cation, which effectively reduced ionic loss by increasing the transition state energy required for the ring distortions, thereby decreasing degradation pathways such as Hofmann β -elimination.

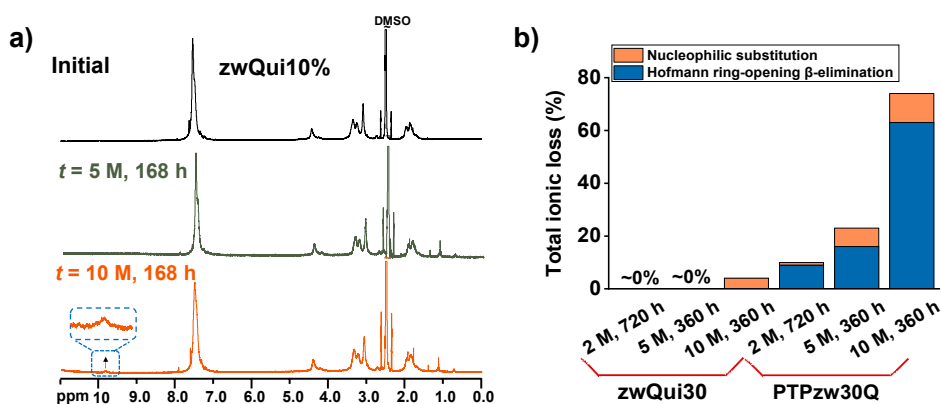


Figure 24. Alkaline stability of the zwQui30% membrane after 168 h storage in 5 and 10 M aq. NaOH at 90 °C (a), and total ionic loss comparison with PTPzw30Q¹⁵⁴ after alkaline treatment in 2 M, aq. NaOH for 720 h and in 5, and 10 M, aq. NaOH for 168 h at 90 °C (b).

5 Conclusion and outlook

5.1 Conclusion

This thesis mainly focused on preparing ether-free polymeric structures through superacid-mediated polyhydroxyalkylation. This method is an efficient way to synthesize high molecular weight polymers with precisely defined structures. In superacidic media, the reaction between ketones and arenes demonstrates broad compatibility with a wide range of monomers, allowing for the fabrication of polymers using both commercially available and newly designed monomers. In total, 29 AEMs were synthesized, the membranes were cast, and the different properties were characterized.

Most of the previously published papers that investigated the alkaline stability of benzylic tethered QA were based on monomers, which inspired us to design the first paper. In Paper I, the placement of QAs on the benzylic positions of ether-free polymer structure and its effects on the alkaline stability were investigated. It was found that the stability of QA tethered at benzylic positions is not only dependent on the structure of QA but also depends on the alkaline concentration, since at lower concentrations, the degradation mainly involved nucleophilic substitution at benzylic sites, while higher concentrations triggered additional pathways, like ring-opening and methyl substitution. In Paper II, the influence of arene configuration, quaterphenyl, on the different properties of AEMs without altering the IEC was investigated. Increasing the proportion of meta-connectivity showed a gradual increase in ionic clustering, water uptake, and hydroxide conductivity in the AEMs. In Paper III, it was found that tethering dual DMP groups via a methylene spacer in fluorene monomer could significantly improve the alkaline stability of AEMs. Furthermore, the IEC was tuned by controlling the monomer feeding ratio of cationic and non-ionic monomers, which affected conductivity and water uptake. The high alkaline stability reported for Spiroionenes, motivated the synthesis of a dispirocyclic QA monomer, DSpI, as the arene to be polymerized with isatin for Paper IV. The IEC of the polymer could be tuned through copolymerization with a non-ionic monomer. The samples showed acceptable stability in 1 M aq. NaOH, however, at 2 M aq. NaOH showed degradation. The high alkaline stability of quinuclidone inspired the synthesis of a series of zwitterionic polymers with precisely controlled ratios of cationic and zwitterionic groups in Paper V. The membranes exhibited high hydroxide conductivity, which decreased as zwitterionic content increased due to reduced water uptake and IEC value while showing high alkaline stability.

5.2 Outlook

While this thesis does not include *in-situ* evaluation data, some *ex-situ* data showed potential for future testing in WEs and FCs. There are some points to be considered for further development in the future. Reducing membrane thickness to 5–30 μm could enhance water management and device longevity, especially for FCs. Future development should explore diverse polymeric structures based on more stable cationic groups like quinuclidinium, improve mechanical properties through reinforcements, and optimize polymerization to increase the molecular weight of polymers. Additionally, continued focus on stability and conductivity development will likely improve durability, ultimately leading to viable commercially available options.

6 References

- (1) <https://unfccc.int/process-and-meetings/the-paris-agreement>. There is no corresponding record for this reference., (accessed 2023-07-27).
- (2) Pollet, B. G.; Kocha, S. S.; Staffell, I. *Curr. Opin. Electrochem.* **2019**, *16*, 90-95.
- (3) M. Hren; M. Božič; D. Fakin; K.S. Kleinschek; Gorgieva, S. *Sustainable Energy Fuels* **2021**, *5* (3), 604-637.
- (4) Das, G.; Choi, J. H.; Nguyen, P. K. T.; Kim, D. J.; Yoon, Y. S. *Polymers (Basel)* **2022**, *14* (6). From NLM PubMed-not-MEDLINE.
- (5) Ghorui, U. K.; Sivaguru, G.; Teja, U. B.; M, A.; Ramakrishna, S.; Ghosh, S.; Dalapati, G. K.; Chakraborty, S. *ACS Appl. Energy Mater.* **2024**, *7* (18), 7649-7676.
- (6) Rolo, I.; Costa, V. A. F.; Brito, F. P. *Energies* **2023**, *17* (1).
- (7) Yang, Y.; Li, P.; Zheng, X.; Sun, W.; Dou, S. X.; Ma, T.; Pan, H. *Chem. Soc. Rev.* **2022**, *51* (23), 9620-9693. From NLM PubMed-not-MEDLINE.
- (8) Chen, H.; Tao, R.; Bang, K. T.; Shao, M.; Kim, Y. *Adv. Energy Mater.* **2022**, *12* (28), 2200934.
- (9) Merle, G., Wessling, Matthias, Nijmeijer, Kitty. *J. Membr. Sci.* **2011**, *377* (1-2), 1-35.
- (10) Mekhilef, S.; Saidur, R.; Safari, A. *Renew. Sust. Energ.* **2012**, *16* (1), 981-989.
- (11) Kreuer, K. D. *Fuel Cells*; Springer: New York 2012.
- (12) Carrette, L.; Friedrich, K. A.; Stimming, U. *ChemPhysSchem.* **2000**, *1* (4), 162-193. From NLM PubMed-not-MEDLINE.
- (13) Mekhilef, S., Saidur, R., Safari, A. *Renew. Sustain. Energy Rev.* **2012**, *16* (1), 981-989.
- (14) Xu, F.; Li, Y.; Ding, J.; Lin, B. *ChemElectroChem* **2023**, *10* (24).
- (15) Ramaswamy, N.; Mukerjee, S. *Chem Rev* **2019**, *119* (23), 11945-11979. From NLM PubMed-not-MEDLINE.
- (16) Zhang, L.; Chae, S.-R.; Hendren, Z.; Park, J.-S.; Wiesner, M. R. *Chemical Engineering Journal* **2012**, *204-206*, 87-97.
- (17) Zaidi, S. J., Takeshi Matsuura. *Polymer Membranes for Fuel Cells Book*; New York: Springer, 2009.
- (18) Jiang, S.; Sun, H.; Wang, H.; Ladewig, B. P.; Yao, Z. *Chemosphere* **2021**, *282*, 130817.
- (19) Henkensmeier, D.; Cho, W. C.; Jannasch, P.; Stojadinovic, J.; Li, Q.; Aili, D.; Jensen, J. O. *Chem Rev* **2024**, *124* (10), 6393-6443. From NLM PubMed-not-MEDLINE.
- (20) Ma, L.; Sui, S.; Zhai, Y. *International Journal of Hydrogen Energy* **2009**, *34* (2), 678-684.
- (21) Liu, R. T.; Xu, Z. L.; Li, F. M.; Chen, F. Y.; Yu, J. Y.; Yan, Y.; Chen, Y.; Xia, B. Y. *Chem Soc Rev* **2023**, *52* (16), 5652-5683. From NLM PubMed-not-MEDLINE.
- (22) Zhang, Y.; Zheng, L.; Liu, B.; Wang, H.; Shi, H. *Journal of Membrane Science* **2019**, *584*, 173-180.

- (23) Schwenzer, B.; Zhang, J.; Kim, S.; Li, L.; Liu, J.; Yang, Z. *ChemSusChem* **2011**, *4* (10), 1388-1406. From NLM Medline.
- (24) T. Wang; J.Y. Jeon; J. Han; J.H. Kim; C. Bae; Kim, S. *J. Membr. Sci.* **2020**, *598*, 117665.
- (25) Hagesteijn, K. F. L.; Jiang, S.; Ladewig, B. P. *J. Mater. Sci.* **2018**, *53*, 11131-11150.
- (26) Hickner, M. A.; Herring, A. M.; Coughlin, E. B. *Journal of Polymer Science Part B: Polymer Physics* **2013**, *51* (24), 1727-1735.
- (27) Grove, W. R. *The London, Edinburgh, and Dublin Philosophical Magazine and Journal of Science* **1839**, *15* (96), 287-293.
- (28) Grove, W. R. *The London, Edinburgh, and Dublin Philosophical Magazine and Journal of Science* **1839**, *14* (86-87), 127-130.
- (29) Sandstede, G.; Cairns, E. J.; Bagotsky, V. S., & Wiesener, K. *History of low temperature fuel cells*; 2010.
- (30) Stambouli, A. B.; Enrico Traversa. *Renew. Sustain. Energy Rev.* **2002**, *6* (3), 295-304.
- (31) Luo, Y.; Wu, Y.; Li, B.; Mo, T.; Li, Y.; Feng, S.-P.; Qu, J.; Chu, P. K. *Journal of Energy Storage* **2021**, *42*.
- (32) Wilberforce, T.; Alaswad, A.; Palumbo, A.; Dassisti, M.; Olabi, A. G. *International Journal of Hydrogen Energy* **2016**, *41* (37), 16509-16522.
- (33) Ajanovic, A.; Haas, R. *Fuel Cells* **2019**, *19* (5), 515-529.
- (34) Thomas, C. E. *International Journal of Hydrogen Energy* **2009**, *34* (15), 6005-6020.
- (35) Guaitolini, S. V. M.; Fardin, J. F. Fuel Cells: History (Short Remind), Principles of Operation, Main Features, and Applications. In *Advances in Renewable Energies and Power Technologies*, 2018; pp 123-150.
- (36) Sharaf, O. Z.; Orhan, M. F. *Renewable Sustainable Energy Rev.* **2014**, *32*, 810-853.
- (37) Boysen, D. A.; Uda, T.; Chisholm, C. R.; Haile, S. M. . *Science* **2004**, *303* (5654), 68-70.
- (38) Sammes, N.; Bove, R.; Stahl, K. *Current Opinion in Solid State and Materials Science* **2004**, *8* (5), 372-378.
- (39) Minh, N. *Solid State Ionics* **2004**, *174* (1-4), 271-277.
- (40) Kulkarni, A.; Giddey, S. *Journal of Solid State Electrochemistry* **2012**, *16* (10), 3123-3146.
- (41) McLean, G. F.; Niet, T.; Prince-Richard, S.; Djilali, N. *Int. J. Hydrog. Energy* **2002**, *27* (5), 507-526.
- (42) Dekel, D. R. *J. Power Sources* **2018**, *375*, 158-169.
- (43) Pan, M.; Pan, C.; Li, C.; Zhao, J. *Renewable and Sustainable Energy Reviews* **2021**, *141*.
- (44) Collin, A.; Kumar, V. B.; Karthikeyan, S.; Sankar, M. G. *Next Energy* **2024**, *5*.
- (45) Hu, X.; Yang, B.; Ke, S.; Liu, Y.; Fang, M.; Huang, Z.; Min, X. *Energy & Fuels* **2023**, *37* (16), 11532-11566.
- (46) Mohideen, M. M.; Radhamani, A. V.; Ramakrishna, S.; Wei, Y.; Liu, Y. *Journal of Energy Chemistry* **2022**, *69*, 466-489.

- (47) Kusoglu, A.; Weber, A. Z. *Chem Rev* **2017**, *117* (3), 987-1104. From NLM PubMed-not-MEDLINE.
- (48) Slade, S., Campbell, S.A., Ralph, T.R. and Walsh, F.C. *J. Electrochem. Soc.* **2002**, *149 A* (1556).
- (49) Jung, H.-Y.; Kim, J. W. *International Journal of Hydrogen Energy* **2012**, *37* (17), 12580-12585.
- (50) Karimi, M. B., Mohammadi, F. Hooshyari, K. *Int. J. Hydrogen Energy*. **2019**, *44* (54), 28919-28938.
- (51) Srinivasan, S. *J. Electrochem. Soc.* **1989**, *136* (2), 41C.
- (52) Ferriday, T. B.; Middleton, P. H. *International Journal of Hydrogen Energy* **2021**, *46* (35), 18489-18510.
- (53) Arges, C. G., Ramani, V. K., Pintauro, P. N. *Electrochem. Soc. Interface* **2010**, *19* (2), 31.
- (54) Pan, Z. F.; An, L.; Zhao, T. S.; Tang, Z. K. *Prog. Energy Combust. Sci.* **2018**, *66*, 141-175.
- (55) Couture, G.; Alaaeddine, A.; Boschet, F.; Ameduri, B. *Prog. Polym. Sci.* **2011**, *36* (11), 1521-1557.
- (56) Varcoe, J. R.; Slade, R. C.; Lam How Yee, E. *Chem Commun (Camb)* **2006**, (13), 1428-1429. From NLM PubMed-not-MEDLINE.
- (57) Huang, J.; Yu, Z.; Tang, J.; Wang, P.; Tan, Q.; Wang, J.; Lei, X. *Int. J. Hydrogen Energy* **2022**, *47* (65), 27800-27820.
- (58) Mandal, M.; Huang, G.; Hassan, N. U.; Peng, X.; Gu, T.; Brooks-Starks, A. H.; Bahar, B.; Mustain, W. E.; Kohl, P. A. *Journal of The Electrochemical Society* **2019**, *167* (5).
- (59) Varcoe, J. R.; Atanasov, P.; Dekel, D. R.; Herring, A. M.; Hickner, M. A.; Kohl, P. A.; Kucernak, A. R.; Mustain, W. E.; Nijmeijer, K.; Scott, K.; et al. *Energy Environ. Sci.* **2014**, *7*, 3135-3191.
- (60) Cheng, J.; He, G.; Zhang, F. *Int. J. Hydrog. Energy* **2015**, *40*, 7348-7360.
- (61) Mustain, W. E., Chatenet, M., Page, M., Kim, Y. S. *Energy Environ. Sci.* **2020**, *13* (9), 2805-2838.
- (62) Li, N.; Guiver, M. D.; Binder, W. H. *ChemSusChem* **2013**, *6* (8), 1376-1383. From NLM Medline.
- (63) Yang, Z.; Ran, J.; Wu, B.; Wu, L.; Xu, T. *Current Opinion in Chemical Engineering* **2016**, *12*, 22-30.
- (64) M.G. Marino, J. P. M., A. Wohlfarth, K.D. Kreuer. *J. Membr. Sci.* **2014**, *464*, 61-71.
- (65) Ludueña, G. A.; Kühne, T. D.; Sebastiani, D. *Chemistry of Materials* **2011**, *23* (6), 1424-1429.
- (66) Marx, D., Chandra, A., Tuckerman, M. E. *Chem. Rev.* *110* (4), 2174-2216.
- (67) Marino, M. G.; Melchior, J. P.; Wohlfarth, A.; Kreuer, K. D. *J. Membr. Sci.* **2014**, *464*, 61-71.
- (68) Agarwal, T.; Prasad, A. K.; Advani, S. G.; Babu, S. K.; Borup, R. L. *J. Mater. Chem. A* **2024**, *12* (24), 14229-14244.

- (69) Arges, C. G.; Parrondo, J.; Johnson, G.; Nadhan, A.; Ramani, V. *J. Mater. Chem. A* **2012**, 22 (9).
- (70) Suzuki, S.; Muroyama, H.; Matsui, T.; Eguchi, K. *Electrochim. Acta* **2013**, 88, 552-558.
- (71) Yue, X. B.; Wang, X. H.; Peng, H.; Lai, L. W.; Zhang, Q. G.; Zhu, A. M.; Liu, Q. L. *J. Membr. Sci.* **2024**, 696.
- (72) Dang, H.-S.; Weiber, E. A.; Jannasch, P. *Journal of Materials Chemistry A* **2015**, 3 (10), 5280-5284.
- (73) Han, J.; Gong, S.; Peng, Z.; Cheng, X.; Li, Y.; Peng, H.; Zhu, Y.; Ren, Z.; Xiao, L.; Zhuang, L. *J. Membr. Sci.* **2021**, 626.
- (74) Dang, H.-S.; Jannasch, P. *ACS Appl. Energy Mater.* **2018**, 1 (5), 2222-2231.
- (75) Dang, H.-S.; Jannasch, P. *Macromolecules* **2015**, 48 (16), 5742-5751.
- (76) Trant, C.; Hwang, S.; Bae, C.; Lee, S. *Macromolecules* **2020**, 53 (19), 8548-8561.
- (77) Clemens, A. L.; Jayathilake, B. S.; Karnes, J. J.; Schwartz, J. J.; Baker, S. E.; Duoss, E. B.; Oakdale, J. S. *Polymers* **2023**, 15 (6). From NLM PubMed-not-MEDLINE.
- (78) Sung, S.; Mayadevi, T. S.; Min, K.; Lee, J.; Chae, J. E.; Kim, T.-H. *Journal of Membrane Science* **2021**, 619.
- (79) Arges, C. G.; Zhang, L. *ACS Appl. Energy Mater.* **2018**, 1, 2991-3012.
- (80) S. Gottesfeld; D.R. Dekel; M. Page; C. Bae; Y. Yan; P. Zelenay; Kim, Y. S. *J. Power Sources* **2018**, 375, 170-184.
- (81) Park, E. J.; Jannasch, P.; Miyatake, K.; Bae, C.; Noonan, K.; Fujimoto, C.; Holdcroft, S.; Varcoe, J. R.; Henkensmeier, D.; Guiver, M. D.; et al. *Chem. Soc. Rev.* **2024**, 53 (11), 5704-5780. From NLM PubMed-not-MEDLINE.
- (82) Miyanishi, S.; Yamaguchi, T. *Phys. Chem. Chem. Phys.* **2016**, 18 (17), 12009-12023. From NLM PubMed-not-MEDLINE.
- (83) Zhang, F.; Li, T.; Chen, W.; Wu, X.; Yan, X.; Xiao, W.; Zhang, Y.; Wang, X.; He, G. *J. Membr. Sci.* **2021**, 624.
- (84) J. R. Varcoe, D. R. D., A. M. Herring, M. A. Hickner, P. A. Kohl, A. R. Kucernak, W. E. Mustain, K. Nijmeijer, K. Scott, T. Xu, L. Zhuang. *Energy Environ. Sci.* **2014**, 7, 3135-3191.
- (85) K. Matsui, E. T., K. Sugimoto, K. Kondo, T. Seita.; Akimoto, A. *J. Appl. Polym. Sci.* **1986**, 32, 4137-4143.
- (86) Zschocke, P., D. Quellmalz. *J. Membr. Sci.* **1985**, 22 (2.3), 325-332.
- (87) Yan, J.; Hickner, M. A. *Macromolecules* **2010**, 43 (5), 2349-2356.
- (88) Zhao, Z.; Wang, J.; Li, S.; Zhang, S. *J. Power Sources* **2011**, 196 (10), 4445-4450.
- (89) Li, N.; Yan, T.; Li, Z.; Thurn-Albrecht, T.; Binder, W. H. *Energy Environ. Sci.* **2012**, 5 (7).
- (90) Danks, T. N.; Slade, R. C. T.; Varcoe, J. R. *J. Mater. Chem. A.* **2002**, 12 (12), 3371-3373.
- (91) Becerra-Arciniegas, R. A.; Narducci, R.; Ercolani, G.; Antonaroli, S.; Sgreccia, E.; Pasquini, L.; Knauth, P.; Di Vona, M. L. *Polymer* **2019**, 185.

- (92) Arges, C. G.; Ramani, V. *Proc. Natl. Acad. Sci. U. S. A.* **2013**, *110* (7), 2490-2495. From NLM Medline.
- (93) Parrondo, J.; Arges, C. G.; Niedzwiecki, M.; Anderson, E. B.; Ayers, K. E.; Ramani, V. *RSC Adv.* **2014**, *4* (19).
- (94) Choe, Y.-K.; Fujimoto, C.; Lee, K.-S.; Dalton, L. T.; Ayers, K.; Henson, N. J.; Kim, Y. S. *Chem. Mat.* **2014**, *26* (19), 5675-5682.
- (95) Mohanty, A. D.; Tignor, S. E.; Krause, J. A.; Choe, Y.-K.; Bae, C. *Macromolecules* **2016**, *49* (9), 3361-3372.
- (96) Lee, W. H.; Mohanty, A. D.; Bae, C. *ACS Macro Lett.* **2015**, *4* (4), 453-457. From NLM PubMed-not-MEDLINE.
- (97) Pham, T. H.; Olsson, J. S.; Jannasch, P. *J. Mater. Chem. A* **2018**, *6*, 16537-16547.
- (98) Olsson, J. S.; Pham, T. H.; Jannasch, P. *J. Membr. Sci.* **2019**, *578*, 183-195.
- (99) A. Allushi; T.H. Pham; J.S. Olsson; Jannasch, P. *J. Mater. Chem. A* **2019**, *7*, 27164-27174.
- (100) Hibbs, M. R.; Fujimoto, C. H.; Cornelius, C. J. *Macromolecules* **2009**, *42* (21), 8316-8321.
- (101) Hibbs, M. R. *J. Polym. Sci. B: Polym. Phys.* **2013**, *51*, 1736-1742.
- (102) Pham, T. H.; Olsson, J. S.; Jannasch, P. *J Am Chem Soc* **2017**, *139* (8), 2888-2891. From NLM PubMed-not-MEDLINE.
- (103) Liu, L.; Li, Q.; Dai, J.; Wang, H.; Jin, B.; Bai, R. *J. Membr. Sci.* **2014**, *453*, 52-60.
- (104) Thomas, O. D.; Soo, K. J. W. Y.; Peckham, T. J.; Kulkarni, M. P.; Holdcroft, S. *Polym. Chem.* **2011**, *2* (8).
- (105) Dang, H. S., P. Jannasch. *J. Mater. Chem. A* **2017**, *5*, 21965-21978.
- (106) Zhang, B.; Gu, S.; Wang, J.; Liu, Y.; Herring, A. M.; Yan, Y. *RSC Adv.* **2012**, *2* (33).
- (107) Kumari, M.; Douglin, J. C.; Dekel, D. R. *J. Membr. Sci.* **2021**, *626*.
- (108) Gu, S.; Wang, J.; Kaspar, R. B.; Fang, Q.; Zhang, B.; Bryan Coughlin, E.; Yan, Y. *Sci. Rep.* **2015**, *5*, 11668. From NLM PubMed-not-MEDLINE.
- (109) Liu, X.; Xie, N.; Xue, J.; Li, M.; Zheng, C.; Zhang, J.; Qin, Y.; Yin, Y.; Dekel, D. R.; Guiver, M. D. *Nature Energy* **2022**, *7* (4), 329-339.
- (110) You, W.; Noonan, K. J. T.; Coates, G. W. *Prog. Polym. Sci.* **2020**, *100*, 101177.
- (111) Vijayakumar, V.; Nam, S. Y. *Journal of Industrial and Engineering Chemistry* **2019**, *70*, 70-86.
- (112) Willdorf-Cohen, S.; Kaushansky, A.; Dekel, D. R.; Diesendruck, C. E. *J Phys Chem Lett* **2022**, *13*, 10216-10221. From NLM Medline.
- (113) Dekel, D. R.; Willdorf, S.; Ash, U.; Amar, M.; Pusara, S.; Dhara, S.; Srebnik, S.; Diesendruck, C. E. *J. Power Sources* **2018**, *375*, 351-360.
- (114) Mohanty, A. D.; Bae, C. *J. Mater. Chem. A* **2014**, *2*, 17314-17320.
- (115) Marino, M. G.; Kreuer, K. D. *ChemSusChem* **2015**, *8* (3), 513-523. From NLM Medline.
- (116) W.H. Lee, E. J. P., J. Han, D.W. Shin, Y.S. Kim, C. Bae. *ACS Macro Lett.* **2017**, *6*, 566-570.

- (117) Li, J.; Yang, C.; Wang, S.; Xia, Z.; Sun, G. *RSC Adv.* **2022**, *12*, 26542-26549.
- (118) Chen, N.; Jin, Y.; Liu, H.; Hu, C.; Wu, B.; Xu, S.; Li, H.; Fan, J.; Lee, Y. M. *Angew Chem Int Ed Engl* **2021**, *60* (35), 19272-19280. From NLM PubMed-not-MEDLINE.
- (119) J.S. Olsson; T.H. Pham; Jannasch, P. *Adv. Funct. Mater.* **2018**, *28*, 1702758.
- (120) Huang, S.; He, X.; Cheng, C.; Zhang, F.; Guo, Y.; Chen, D. *Int. J. Hydrogen Energy.* **2020**, *45* (23), 13068-13079.
- (121) Lu, J.; Wang, Y.; Li, J.; Zhao, J.; Lei, Y.; Gao, J.; Li, W.; Sun, S.; Wang, Z. *J. Power Sources* **2024**, 624.
- (122) Cheng, X.; Li, C.; Zou, X.; Wang, W.; Meng, X. *Sep. Purif. Technol.* **2024**, 345.
- (123) Zhang, J.; Zhang, K.; Liang, X.; Yu, W.; Ge, X.; Shehzad, M. A.; Ge, Z.; Yang, Z.; Wu, L.; Xu, T. *J. Mater. Chem. A* **2021**, *9* (1), 327-337.
- (124) Huang, G.; Mandal, M.; Peng, X.; Yang-Neyerlin, A. C.; Pivovar, B. S.; Mustain, W. E.; Kohl, P. A. *J. Electrochem. Soc.* **2019**, *166* (10), F637-F644.
- (125) Konovalova, A.; Kim, H.; Kim, S.; Lim, A.; Park, H. S.; Kraglund, M. R.; Aili, D.; Jang, J. H.; Kim, H.-J.; Henkensmeier, D. *J. Membr. Sci.* **2018**, *564*, 653-662.
- (126) Mustain, W. E.; Chatenet, M.; Page, M.; Kim, Y. S. *Energy Environ. Sci.* **2020**, *13*, 2805-2838.
- (127) Xia, L.; Holtwerth, S.; Rodenbücher, C.; Lehnert, W.; Shviro, M.; Müller, M. *J. Power Sources* **2024**, 590 233802.
- (128) Zhang, Y.; Parrondo, J.; Sankarasubramanian, S.; Ramani, V. *ChemSusChem* **2017**, *10* (15), 3056-3062. From NLM Medline.
- (129) Olah, G. A. *Angew. Chem.* **1993**, *32* (6), 767 - 922.
- (130) Olah, G. A., Rasul, G., York, C., Prakash, G. S. *J. Am. Chem. Soc.* **1995**, *117* (45), 11211-11214.
- (131) Rusanov, A. L.; Chebotarev, V. P.; Lovkov, S. S. *Russian Chemical Reviews* **2008**, *77* (6), 547-553.
- (132) Gasonoo, M.; Sumita, A.; Boblak, K. N.; Giuffre, K.; Ohwada, T.; Klumpp, D. A. *J Org Chem* **2017**, *82* (12), 6044-6053. From NLM PubMed-not-MEDLINE.
- (133) Colquhoun, H. M., Zolotukhin, M. G., Khalilov, L. M., Dzhemilev, U. M. *Macromolecules* **2001**, *34* (4), 1122-1124.
- (134) M.T. Guzmán-Gutiérrez; D.R. Nieto; S. Fomine; S.L. Morales; M.G. Zolotukhin; M.C.G. Hernandez; H. Kricheldorf; Wilks, E. S. *Macromolecules* **2010**, *44*, 194-202.
- (135) Segawa, Y., Higashihara, T., Ueda, M. *J. Am. Chem. Soc.* **2010**, *132* (32), 11000-11001.
- (136) Ryu, T.; Jang, H.; Ahmed, F.; Lopa, N. S.; Yang, H.; Yoon, S.; Choi, I.; Kim, W. *International Journal of Hydrogen Energy* **2018**, *43* (10), 5398-5404.
- (137) Pan, D.; Chen, S.; Jannasch, P. *ACS Macro Lett* **2023**, *12* (1), 20-25. From NLM Medline.
- (138) Diaz, A. M.; Zolotukhin, M. G.; Fomine, S.; Salcedo, R.; Manero, O.; Cedillo, G.; Velasco, V. M.; Guzman, M. T.; Fritsch, D.; Khalizov, A. F. *Macromolecular Rapid Communications* **2007**, *28* (2), 183-187.

- (139) Li, X.; Yang, K.; Li, Z.; Guo, J.; Zheng, J.; Li, S.; Zhang, S.; Sherazi, T. A. *International Journal of Hydrogen Energy* **2022**, 47 (33), 15044-15055.
- (140) Lira, A. L.; Zolotukhin, M. G.; Fomina, L.; Fomine, S. *Macromolecular Theory and Simulations* **2007**, 16 (3), 227-239.
- (141) L.I. Olvera, M. T. G.-G., M.G. Zolotukhin, S. Fomine, J. Cárdenas, F.A. Ruiz-Trevino, D. Villers, T.A. Ezquerro, E. Prokhorov. *Macromolecules* **2013**, 46 (18), 7245–7256.
- (142) Klumpp, D. A., Garza, M., Jones, A., Mendoza, S. *J. Org. Chem.* **1999**, 64 (18), 6702-6705.
- (143) Yang, D., Yip, Y. C., Jiao, G. S., Wong, M. K. . *J. Org. Chem.* **1998**, 63 (24), 8952-8956.
- (144) Geneste, P., Durand, R., Hugon, I., Reminiac, C. *J. Org. Chem.* **1979**, 44 (12), 1971-1973.
- (145) Sinananwanich, W., Higashihara, T., Ueda, M. *Macromolecules* **2009**, 42 (4), 994-1001.
- (146) Conroy, J. L., Sanders, T. C., Seto, C. T. *J. Am. Chem. Soc.* **1997**, 119 (18), 4285-4291.
- (147) Xu, F.; Chen, Y.; Cao, X.; Li, J.; Lin, B.; Yuan, N.; Ding, J. *Journal of Power Sources* **2022**, 545.
- (148) He, X.; Feng, H.; Wen, J.; Su, Q.; Wang, X.; Cai, Z.; Qian, Y.; Zhang, H.; Li, M. *Int. J. Hydrogen Energy*. **2024**, 86, 808-814.
- (149) Wen, J.; He, X.; Zhang, G.; Zeng, M.; Qian, Y.; Li, M. *Science China Materials* **2024**, 67 (3), 965-973.
- (150) A. Allushi; T.H. Pham; Jannasch, P. *J. Membr. Sci.* **2021**, 632, 119376.
- (151) Miyaura, N., Akira Suzuki *Chem. Rev.* **1995**, 95 (7), 2457-2483.
- (152) Oh, S.-H.; Na, S.-I.; Nah, Y.-C.; Vak, D.; Kim, S.-S.; Kim, D.-Y. *Organic Electronics* **2007**, 8 (6), 773-783.
- (153) Yin, L.; Ren, R.; He, L.; Zheng, W.; Guo, Y.; Wang, L.; Lee, H.; Du, J.; Li, Z.; Tang, T.; et al. *Angew. Chem., Int. Ed. Engl.* **2024**, 63 (19), e202400764. From NLM PubMed-not-MEDLINE.
- (154) Shirole, A.; Bakvand, P. M.; Jannasch, P. *ACS Appl. Energy Mater.* **2023**, 6 (13), 7240-7249.
- (155) Lu, C.; Long, C.; Li, Y.; Li, Z.; Zhu, H. *J. Membr. Sci.* **2020**, 598.
- (156) Wang, J.; Zhao, Y.; Setzler, B. P.; Rojas-Carbonell, S.; Ben Yehuda, C.; Amel, A.; Page, M.; Wang, L.; Hu, K.; Shi, L.; et al. *Nat. Energy* **2019**, 4, 392-398.
- (157) T.H. Pham; A. Allushi; J.S. Olsson; Jannasch, P. *Polym. Chem.* **2020**, 11, 6953-6963.
- (158) Qiao, X.; Wang, X.; Liu, S.; Shen, Y.; Li, N. *J. Membr. Sci.* **2021**, 630.
- (159) Li, Y.; Lin, X.; Wu, L.; Jiang, C.; Hossain, M. M.; Xu, T. *J. Membr. Sci.* **2015**, 483, 60-69.
- (160) Irfan, M.; Xu, T.; Ge, L.; Wang, Y.; Xu, T. *J. Membr. Sci.* **2019**, 588.

- (161) Cassegrain, S.; Saatkamp, T.; Mardle, P.; Gangrade, A.; Hui, J.; Holdcroft, S. *Chem. Mater.* **2023**, *36* (1), 197-210.
- (162) Yang, P. X.; Wang, J.; Liu, H. L.; Guo, Z. Y.; Huang, Z. H.; Zhang, P. P.; Ji, Z. Y. *ACS Appl. Mater. Interfaces.* **2024**, *16* (27), 35576-35587. From NLM PubMed-not-MEDLINE.

